Fine Tuning of Photophysical Properties of *meso*–*meso*-Linked Zn^{II}–Diporphyrins by Dihedral Angle Control

Naoya Yoshida,[a] Tomoya Ishizuka,[a] Atsuhiro Osuka,*[a] Dae Hong Jeong,[b] Hyun Sun Cho,[b] Dongho Kim,*[b] Yoichi Matsuzaki,[c] Atsushi Nogami,[c] and Kazuyoshi Tanaka[d]

Abstract: A series of *meso*–*meso*-linked diporphyrins $\mathbf{S}_n$ strapped with a dioxymethylene group of various length were synthesized by intramolecular Ag^I-promoted coupling of dioxymethylene-bridged diporphyrins $\mathbf{B}_n$, for $n = 10$, 8, 6, 5, 4, 3, 2, and 1. Shortening of the strap length causes a gradual decrease in the dihedral angle between the porphyrins and increasing distortion of porphyrin ring, as suggested by MM2 calculations and ^{1}H NMR studies. This trend has been also suggested by X-ray crystallographic studies on the corresponding Cu^{II} complexes of nonstrapped diporphyrin **2Cu**, and strapped diporphyrins $\mathbf{S_8Cu}$, $\mathbf{S_4Cu}$, and $\mathbf{S_2Cu}$. The absorption spectrum of relatively unconstrained diporphyrins $\mathbf{S_{10}}$ strapped with a long chain exhibits split Soret bands at 414 and 447 nm and weak Q(0,0)- and prominent Q(1,0)-bands, both of which are similar to those of nonstrapped diporphyrin **2**. Shortening of the strap length causes systematic changes in the absorption spectra, in which the intensities of the split Soret bands decrease, the absorption bands at about 400 nm and > 460 nm increase in intensity, and a prominent one-band feature of a Q-band is changed to a distinct two-band feature with concurrent progressive red-shifts of the lowest Q(0,0)-band. The fluorescence spectra also exhibit systematic changes, roughly reflecting the changes of the absorption spectra. The strapped diporphyrins $\mathbf{S}_n$ are all chiral and have been separated into enantiomers over a chiral column. The CD spectra of the optically active $\mathbf{S}_n$ display two Cotton effects at 430–450 and at about 400 nm with the opposite signs. The latter effect can be explained in terms of oblique arrangement of $\boldsymbol{m}_{\perp 1}$ and $\boldsymbol{m}_{\perp 2}$ dipole moments, while the former effect cannot be accounted for within a framework of the exction coupling theory. The resonance Raman (RR) spectra taken for excitation at 457.9 nm are variable among $\mathbf{S}_n$, while the RR spectra taken for excitation at 488.0 nm are constant throughout the $\mathbf{S}_n$ series. These photophysical properties can be explained in terms of INDO/S-SCI calculations, which have revealed charge transfer (CT) transitions accidentally located close in energy to the excitonic Soret transitions. This feature arises from a close proximity of the two porphyrins in *meso*–*meso*-linked diporphyrins. In addition to the gradual red-shift of the exciton split Soret band, the calculations predict that the high-energy absorption band at about 400 nm, the lower energy Cotton effect, and the RR spectra taken for excitation at 457.9 nm are due to the CT states which are intensified upon a decrease in the dihedral angle.

Keywords: copper · fluorescence spectroscopy · porphyrinoids · structure elucidation · zinc

Introduction

Over the last two decades, considerable efforts have been devoted to the synthesis of covalently linked diporphyrins as a minimum functional unit for catalysts for the four-electron reduction of oxygen,[1] photosynthetic reaction centers (RC's), and light harvesting complexes (LHC's).[2–6] With these diporphyrins, tuning and optimization of intramolecular

[a] Prof. A. Osuka, Dr. N. Yoshida, T. Ishizuka
Department of Chemistry
Graduate School of Science
Kyoto University
and Core Research for Evolutional Science and Technology (CREST)
of Japan Science and Technology Corporation (JST)
Kyoto 606-8502 (Japan)
Fax: (+81) 75-753-3970
E-mail: osuka@kuchem.kyoto-u.ac.jp

[b] Prof. D. Kim, Dr. D. H. Jeong, H. S. Cho
Department of Chemistry, Yonsei University
Seoul 120-749 (Korea)

[c] Y. Matsuzaki, Dr. A. Nogami
Japan Advanced Technology Research Laboratories
Nippon Steel Corporation, 20-1 Shintomi, Futtsu
Chiba 293-8511 (Japan)

[d] Prof. K. Tanaka
Department of Molecular Engineering
Graduate School of Engineering, Kyoto University
Sakyo-ku, Kyoto 606-8501 (Japan)

Supporting information for this article is available on the WWW under http://www.chemeuj.org or from the author: Structural parameters of strapped free base diporphyrins calcualted by MM2, 500 MHz ^{1}H NMR spectra of **2**, $\mathbf{S_8}$, $\mathbf{S_6}$, $\mathbf{S_4}$, $\mathbf{S_2}$, and $\mathbf{S_1}$ in aromatic region, emission spectra of **2** and $\mathbf{S}_n$ at 77 K in 2-methyltetrahydrofuran, and the CD spectra of opically pure $\mathbf{S}_n$.

0947-6539/03/0901-0058 $ 20.00+.50/0 *Chem. Eur. J.* **2003**, *9*, No. 1

electron- and/or energy-transfer processes have been examined by varying the interporphyrin distance, orientation, and the electronic property of a bridge.[4–7] Whereas the distance dependence has been rather actively examined to reveal the electronic-exchange-mediating ability of a bridge,[5] the orientation dependence remains only poorly explored, mostly due to synthetic difficulties of models pertinent for such a purpose.[6, 7] We have reported the orientation-dependent exciton coupling of Zn^{II} diporphyrins bridged by naphthalene spacers,[8a] which were also useful for the examination of the geometry dependence of intramolecular energy- and electron-transfer procress.[9] In recent years, the large molecular coefficients of the Soret band in Zn^{II} porphyrins have been used as a tool for the determination of the absolute stereochemistry of chiral molecules owing to effective exciton-coupled circular dichroism.[10]

Recently, we found that Ag^{I}-salt-promoted oxidation of a 5,15-diaryl Zn^{II} porphyrin led to the synthesis of a *meso*–*meso*-linked diporphyrin, in which the Soret band is largely split by exciton coupling owing to a large oscillator strength and a short 8.35 Å center-to-center distance between the two porphyrins.[11, 12] It has been further revealed that this coupling reaction can be extended effectively to higher discrete oligomers (the longest one reported is a 128-mer), all of which display the absorption spectra that can be qualitatively accounted for in terms of the exciton coupling theory.[11d,g, 13] These arrays may be potentially interesting as an optical wire, in that 1) they are linear rod-like shape, 2) the close proximity of the two porphyrins provides large electronic interactions and enables efficient energy transfer along the array, and further 3) a discrete array with defined molecular length determined by the number of porphyrins can be easily prepared.[11d]

Another key feature of this system is *an orthogonal conformation* of the neighboring porphyrins; this provides good solubilities of the arrays, possibly preventing $\pi-\pi$ stacking. This is quite important in the manipulation of very long arrays. In addition, the orthogonal conformation disrupts interporphyrin π-conjugation, hence enabling a very rapid state-to-state energy- or electron-transfer process with avoidance of electronic full delocalization, even in the very proximate situation. Actually we have observed a rapid energy transfer in a *meso*–*meso*-linked $zinc^{II}$/free-base hybrid diporphyrin with a rate of 0.56 ps^{-1}.[14]

With these backgrounds, systematic control of the dihedral angle of the *meso*–*meso*-coupled diporphyrins is an intriguing challenge, since it may offer a fine tuning of electronic interactions between the two porphyrins; this may eventually result in control of intramolecular excitation-energy- and electron-transfer processes. The electronic interaction between the *meso*–*meso*-linked diporphyrins is considered to be minimum at 90° dihedral angle. Therefore, tilting of a porphyrin ring from 90° to $<90°$ causes a symmetry change from D_{2d} to D_2 with a simultaneous increase in the electronic interactions between the porphyrins; this may, in turn, influence the absorption and fluorescence properties depending on the degree of induced enhancement of the electronic interactions. When the electronic interaction is large enough to give rise to full delocalization of the diporphyrin orbitals, a state-to-state energy- or electron-transfer may become no longer feasible.

In this paper, we report the synthesis, X-ray structures, and optical and electrochemical characterizations of a series of strapped *meso*–*meso*-linked diporphyrins in which the dihedral angle of the diporphyrins is systematically changed by introducing a dioxymethylene strap varying the number of carbon atoms ($n=10$, 8, 6, 5, 4, 3, 2, and 1; see Scheme 1)

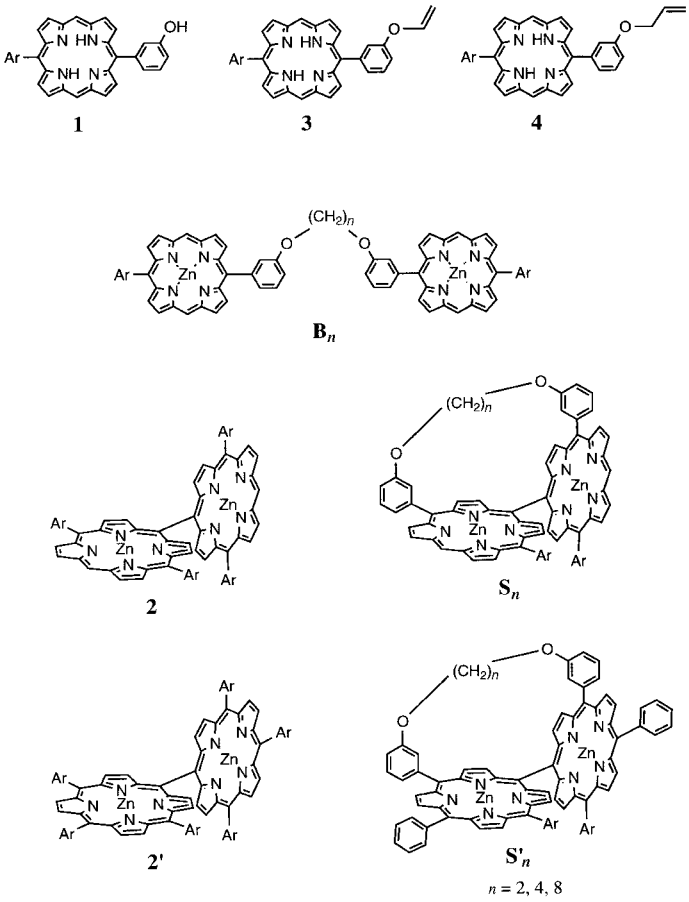

Scheme 1. Ar = 3,5-di-*t*ert-butylphenyl; $n=10$, 8, 6, 5, 4, 3, 2, and 1 for $\mathbf{B}_n$ and $\mathbf{S}_n$.

between the two porphyrins, with a particular concern on the dependence of the absorption spectra of strapped Zn^{II} diporphyrins upon the dihedral angle.[15] In the last part, the molecular orbitals of the strapped diporphyrins have been investigated on the basis of the INDO/S calculation to provide a rational explanation for the dihedral angle dependence of the absorption spectra.

Results

Synthesis: Decamethylene-1,10-dioxy-bridged diporphyrin $\mathbf{B_{10}}$ was prepared in 86% isolated yield by Williamson reaction of 5-(3,5-di-*tert*-butylphenyl)-15-(3-hydroxyphenyl)-porphyrin (**1**) with 1,10-dibromodecane (K_2CO_3, acetone) in acetone followed by zinc insertion. Similar reactions of **1** with longer dihaloalkanes ($n=8$, 6, 5, 4, and 3) gave bridged dimers

  0947-6539/03/0901-0059 $ 20.00+.50/0

$\mathbf{B_8}$, $\mathbf{B_6}$, $\mathbf{B_5}$, $\mathbf{B_4}$, and $\mathbf{B_3}$ in good yields (61–92%), while the reactions with shorter dihaloalkanes ($n=2$ and 1) gave bridged dimers $\mathbf{B_2}$ and $\mathbf{B_1}$ only in poor yields (Table 1). In the preparation of $\mathbf{B_2}$, elimination side product **3** was formed

Table 1. Syntheses of $\mathbf{B}_n$ and $\mathbf{S}_n$.[a]

n	$\mathbf{B}_n$		$\mathbf{S}_n$
	1,ω-dihaloalkane	Product (Yield [%])	Product (Yield [%])
10	$Br(CH_2)_{10}Br$	$\mathbf{B_{10}}$ (86)[b]	$\mathbf{S_{10}}$ (68)
8	$I(CH_2)_8I$	$\mathbf{B_8}$ (82)[b]	$\mathbf{S_8}$ (65)
6	$I(CH_2)_6I$	$\mathbf{B_6}$ (83)[b]	$\mathbf{S_6}$ (60)
5	$Br(CH_2)_5Br$	$\mathbf{B_5}$ (70)[b]	$\mathbf{S_5}$ (43)
4	$Br(CH_2)_4Br$	$\mathbf{B_4}$ (92)[b]	$\mathbf{S_4}$ (63)
3	$Br(CH_2)_3Br$	$\mathbf{B_3}$ (61)[b]	$\mathbf{S_3}$ (38)
2	$Br(CH_2)_2Br$	$\mathbf{B_2}$ (13)[b]	
	$Br(CH_2)_2Br$	$\mathbf{B_2}$ (40)[c]	$\mathbf{S_2}$ (35)
1	$BrCH_2Br$	$\mathbf{B_1}$ (12)[b]	
	$BrCH_2Br$	$\mathbf{B_1}$ (84)[c]	$\mathbf{S_1}$ (20)

[a] Numbers in the parentheses are the isolated yields of products. [b] In acetone. [c] In DMF.

in a substantial amount and the poor solubility of $\mathbf{B_2}$ made its separation further difficult. The similar elimination product **4** was also formed in the preparation of $\mathbf{B_3}$. The reaction of **1** with dibromomethane was quite slow, but the product $\mathbf{B_1}$ was easily separated owing to the absence of an elimination side product. In the meantime, we found that the use of dipolar DMF as solvent improved the yields of $\mathbf{B_2}$ and $\mathbf{B_1}$. With a set of $\mathbf{B}_n$ ($n=10$, 8, 6, 5, 4, 3, 2, and 1) in hand, we examined their intramolecular Ag^I-promoted *meso*–*meso* coupling reaction. To suppress the intermolecular coupling, the reaction of $\mathbf{B}_n$ was carried out at about 10^{-4} M concentration, rather dilute conditions in comparison with the concentration (about 2×10^{-3} M) used for the intermolecular coupling reactions.[11] The reaction of $\mathbf{B_{10}}$ with $AgPF_6$ gave strapped diporphyrin $\mathbf{S_{10}}$ in 68% yields along with the recovery of $\mathbf{B_{10}}$ (17%) and higher oligomers (about 10%) after preparative GPC and silica gel column chromatography. Similarly the reactions of $\mathbf{B_8}$, $\mathbf{B_6}$, $\mathbf{B_5}$, and $\mathbf{B_4}$ afforded strapped diporphyrins $\mathbf{S_8}$, $\mathbf{S_6}$, $\mathbf{S_5}$, and $\mathbf{S_4}$, respectively, in 60–65% isolated yields. It is worth mentioning that diporphyrins $\mathbf{S_3}$–$\mathbf{S_1}$, bearing short straps, were similarly synthesized in moderate yields by the same Ag^I-promoted oxidation despite large strains. As described later, $\mathbf{S_1}$ is most easily oxidized due to its low one-electron oxidation potential and thus quite prone to undergo further coupling. Therefore, in the synthesis of $\mathbf{S_1}$, we used more dilute conditions (4×10^{-5} M) in order to suppress further coupling. Recycling preparative GPC was found to be more convenient than usual chromatography over a silica gel column owing to large differences in exclusion volumes between $\mathbf{B}_n$ and $\mathbf{S}_n$. Under the standard conditions, most of the strapped diporphyrins were stable except the most distorted diporphyrin $\mathbf{S_1}$, which decomposed slowly even at low temperature as revealed in the change in its absorption spectrum. Therefore, all the characterizations of $\mathbf{S_1}$ were done with a fresh sample.

Estimation of diporphyrin strucrures in solution: Structures of the nonstrapped diporphyrin **2** and the strapped diporphyrins $\mathbf{S_{10}}$–$\mathbf{S_1}$ have been estimated by MM2 calculations. With a decrease in the strap length, it is apparent that the torsional strain becomes increased, also giving rise to deformation of porphyrin ring. It has been calculated that the strain is initially accommodated by a decrease in the dihedral angle between the two porphyrins (θ_S and θ_{NS}, in which the suscripts S and NS indicate the strapped and nonstrapped sides, respectively), but eventually becomes too severe for such an accommodation. Then such a large distortion affects other structural parameters including the mean planar deviations (ϕ), the bending angles of the *meso*–*meso* bond with respect to C^{10}–C^{20} or $C^{10'}$–$C^{20'}$ (α), the bending angle of C^{21}–C^{24} with respect to C^5–C^{15} (β), the tilting angle of *meso*-aryl group with respect to the porphyrin plane (δ_S and δ_{NS},), and the *meso*–*meso* bond length (χ) (Supporting Information; for the numbering of carbon atoms, see Figure 3 below). The calculations have indicated that the porphyrin rings in **2**, $\mathbf{S_{10}}$, and $\mathbf{S_8}$ are almost flat with negligible mean plane deviations and arranged roughly in a perpendicular manner with the dihedral angles of 87°, 94°, and 90°, respectively. For the diporphyrins with shorter straps, the dihedral angles have been calculated as follows: 80° ($\mathbf{S_6}$), 77° ($\mathbf{S_5}$), 71° ($\mathbf{S_4}$), 48° ($\mathbf{S_3}$), 42° ($\mathbf{S_2}$), and 36° ($\mathbf{S_1}$). Along with these decreases in the dihedral angles, the structural parameters have been calculated to deviate largely from those of **2**, suggesting the increasing distortions. A rotational barrier around the *meso*–*meso* linkage has been also calculated for simple *meso*–*meso*-linked diporphyrin; this indicates that there is a relatively shallow energy minimum around 90°, but the barrier increases sharply with a decrease in the dihedral angle, preventing a full rotation, in line with our recent finding that the enantiomers of *meso*–*meso*-linked diprophyrin formed from 5,15-substituted Zn^{II} porphyrins were thermally stable.[16] We have also calculated the structures of strapped diporphyrins by the B3LYP hybrid density-functional theory, which also predicts a shallow energy minimum around 90° of the dihedral angle.

^{1}H NMR spectra: The ^{1}H NMR spectra of the diporphyrins were measured in $CDCl_3$ and the chemical shifts of the aromatic protons are listed in Table 2. Assignments have been made on the basis of full 2D-ROESY measurements and the designations of the protons are indicated in Figure 1. The nonstrapped diporphyrin **2** has a signal at $\delta=10.39$ ppm for H^1 and four β-proton signals at $\delta=9.49$ (H^3), 9.18 (H^2), 8.74 (H^6), and 8.12 ppm (H^7), of which the chemical shifts of the outer ones (H^2 and H^3) are almost the same as those of a

Table 2. ^{1}H NMR chemical shifts of porphyrin peripheral protons in **2** and $\mathbf{S_{10}}$–$\mathbf{S_1}$ in $CDCl_3$.

	Outer					Inner			
	H^1	H^2	H^3	H^4	H^5	H^6	H^7	H^8	H^9
2	10.39	9.18	9.49	–	–	8.74	8.12	–	–
$\mathbf{S_{10}}$	10.39	9.21	9.50	9.49	9.20	8.79	8.30	7.95	8.70
$\mathbf{S_8}$	10.39	9.26	9.51	9.50	9.21	8.83	8.42	7.87	8.66
$\mathbf{S_6}$	10.37	9.33	9.50	9.50	9.21	8.89	8.61	7.71	8.62
$\mathbf{S_5}$	10.36	9.38	9.50	9.50	9.23	8.98	8.55	7.60	8.85
$\mathbf{S_4}$	10.36	9.43	9.51	9.50	9.25	9.08	9.22	7.18	8.46
$\mathbf{S_3}$	10.33	9.44	9.48	9.48	9.23	9.12	9.48	6.90	8.34
$\mathbf{S_2}$	10.32	9.45	9.49	9.49	9.24	9.24	9.91	6.32	8.10
$\mathbf{S_1}$	10.31	9.49	9.49	9.49	9.23	9.26	10.08	6.12	8.13

0947-6539/03/0901-0060 $ 20.00+.50/0 *Chem. Eur. J.* **2003**, *9*, No. 1

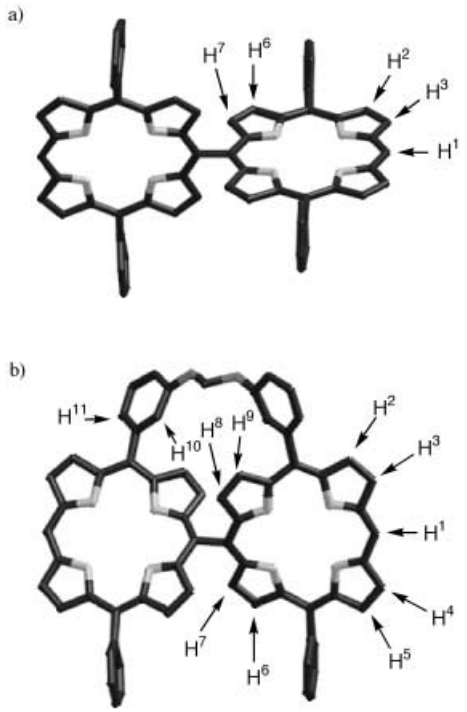

Figure 1. Definitions of proton position numbers of a) **2** and b) $\mathbf{S}_n$ in ^{1}H NMR spectra. *tert*-Butyl groups on phenyl groups are omitted for clarity.

monomeric 5,15-diaryl Zn^{II} porphyrin, while the inner ones (H^6 and H^7) exhibit upfield shifts owing to the ring current effect of the adjacent porphyrin. The peripheral protons of the strapped diporphyrins ($\mathbf{S_{10}}-\mathbf{S_1}$) appear as a singlet for H^1 and eight doublets for the β-protons (H^2-H^9). While the outer β-protons (H^2-H^5) and *meso*-proton H^1 are scarcely affected by changes in the strap length, the inner β-protons (H^6-H^9) show contrasting shifts. Namely, with a decrease in the strap length, the β-protons at the strap-side (H^8 and H^9) are upfield shifted and those at the nonstrapped side (H^6 and H^7) are downfield shifted. Of these, the H^8 and H^7 protons, which lie adjacent to the *meso*–*meso* linkage, exhibit the largest upfield and downfield shifts, respectively; this probably reflects a change in the influence of the neighboring porphyrin ring current, which is sensitive to the dihedral angle between the two porphyrins. This feature, which is enhanced upon the decrease of the strap length, cannot be explained only by symmetric tilting of the two porphyrins, but also by invoking bending of the *meso*–*meso* linkages with respect to $C_{10}-C_{20}$ and $C_{10'}-C_{20'}$ connecting axes. This bending causes the shift of H^8 and H^7 locations to more shielding and deshielding regions, respectively. Similar features are noted for H^9 and H^2 and for H^{10} and H^{11}, but with less magnitude. In both cases, the bisecting phenyl group exerts additional increasing shielding and deshielding effects, respectively, upon the decrease in the strap length. The distortion of the porphyrin ring would increase upon the decrease of the strap, but the fact that the *meso*-protons (H^1) and the outer β-protons (at the nonstrapped side) of $\mathbf{S_{10}}$-$\mathbf{S_1}$ appear almost at the same chemical shifts of **2** indicate that a porphyrin ring current is not seriously affected by the introduction of a short strap, even in the case of $\mathbf{S_1}$, in solution.

X-ray structures of strapped Cu^{II} diporphyrins: In spite of strenuous attempts, X-ray quality crystals were not obtained for the strapped Zn^{II} diporphyrins.[17] Instead, the crystals suitable for X-ray analysis were obtained for Cu^{II} complexes of nonstrapped diporphyrin and several strapped diporphyrins. The X-ray structures of **2Cu**, $\mathbf{S_8Cu}$, $\mathbf{S_4Cu}$, and $\mathbf{S_2Cu}$, which provide useful structural information on the corresponding Zn^{II} diporphyrins, are shown in Figures 2–5. Selected structural parameters are listed in Tables 3 and 4.

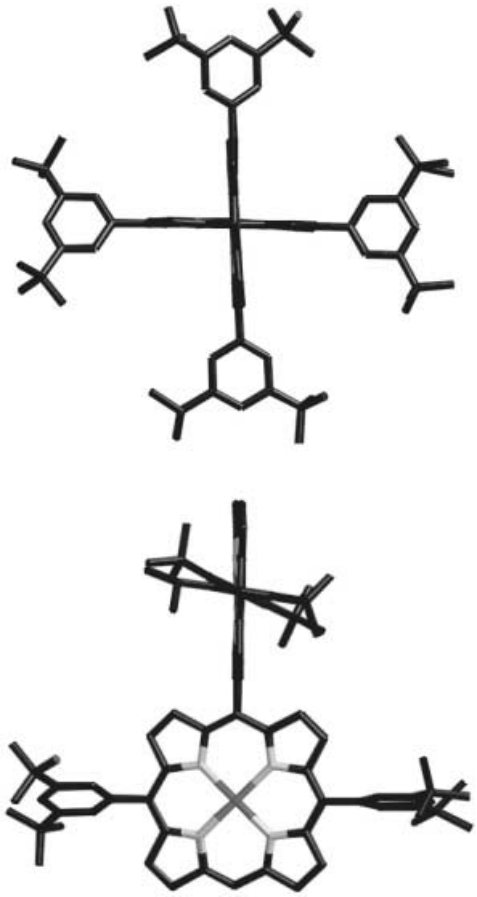

Figure 2. X-ray crystal structure of **2Cu**. Hydrogen atoms and solvents were omitted for clarity.

The X-ray structure of **2Cu** shows two quite planar porphyrin rings with the mean planar deviation (ϕ) of 0.004 Å connected in a perpendicular manner ($\theta_S = 86°$and $\theta_{NS} = 89°$) with a *meso*–*meso* bond length (χ) of 1.51 Å and a Cu–Cu distance of 8.34 Å (Figure 2). The X-ray structure of $\mathbf{S_8Cu}$ exhibits two different ruffled porphyrin rings ($\phi = 0.33$ and 0.35 Å) connected with dihedral angles of $\theta_S = 64.9°$ and $\theta_{NS} = 80°$. The *meso*–*meso* bond length is 1.50 Å and the Cu–Cu distance is 8.40 Å. Small but distinct distortions are apparent from large ϕ values as well as somewhat enhanced α and β values (Table 3). In the crystals of $\mathbf{S_4Cu}$ and $\mathbf{S_2Cu}$, two different diporphyrin structures are found, packed in a pairwise manner. In both cases, the two structures have different structural parameters; we call a structure with a large dihedral angle an A structure and one with a small dihedral angle a B structure. In the case of $\mathbf{S_4Cu}$, the A structure exhibits $\phi = 0.65$

  0947-6539/03/0901-0061 $ 20.00+.50/0

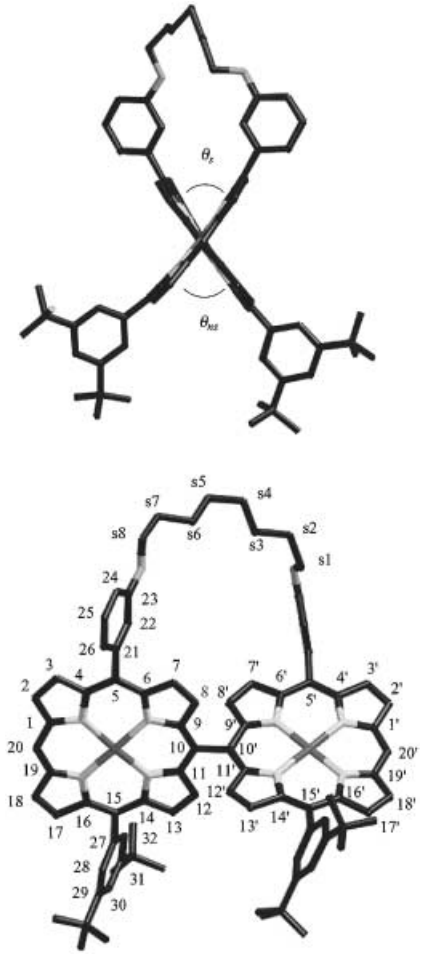

Figure 3. X-ray crystal structure of **S_8Cu**. Hydrogen atoms and solvents were omitted for clarity.

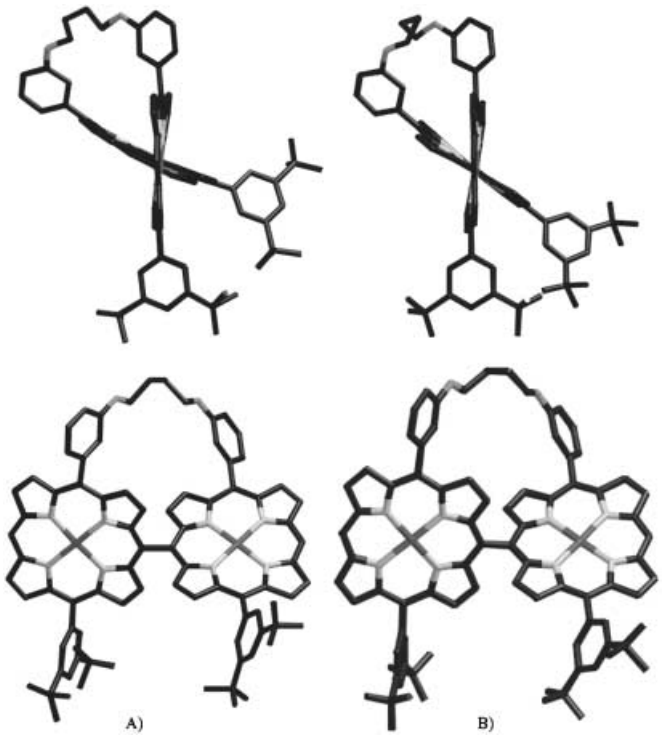

Figure 4. X-ray crystal structure of **S_4Cu** (structures A and B; see text). Hydrogen atoms and solvents were omitted for clarity.

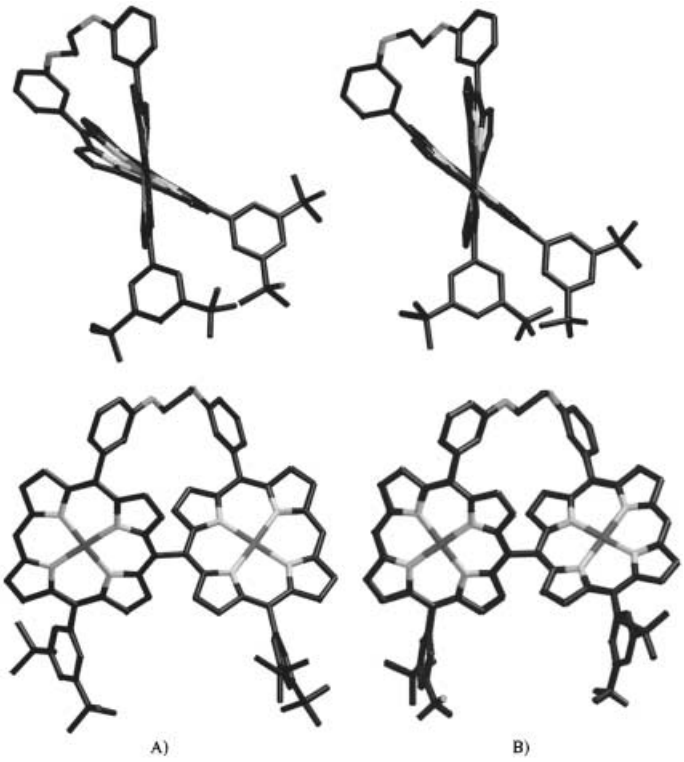

Figure 5. X-ray crystal structure of **S_2Cu** (structures A and B; see text). Hydrogen atoms and solvents were omitted for clarity.

and 0.72 Å, $\theta_S = 60.8°$, $\theta_{NS} = 67.5°$, and $\chi = 1.53$ Å, and the B structure exhibits $\phi = 0.61$ and 0.70 Å, $\theta_S = 53.2°$, $\theta_{NS} = 58.8°$, and $\chi = 1.47$ Å. The A and B structures have the similar mean plane deviations (ϕ), which are larger than those of **2Cu** and **S_8Cu**, but differ in the *meso*–*meso* bond length (χ), which is longer in A and shorter in B in comparison with that of the nonstrapped **2Cu**. In the crystal of **S_2Cu**, the A structure exhibits $\phi = 0.46$ and 1.30 Å, $\theta_S = 50.6°$, $\theta_{NS} = 59.4°$, and $\chi = 1.52$ Å, and the B structure exhibits $\phi = 0.15$ and 1.64 Å, $\theta_S = 50.3°$, $\theta_{NS} = 55.0°$, and $\chi = 1.48$ Å. The structural differences between the two porphyrins in **S_2Cu** are larger compared with those in **S_4Cu**, particularly with respect to the mean plane deviation. Namely, one porphyrin is relatively flat and the other is severely distorted with a large ϕ value. There is a similar trend that the *meso*–*meso* bond length in the diporphyrin conformer with a smaller dihedral angle (B structure) is shorter than that in the other conformer (A structure), but the difference in dihedral angles between the two structures is smaller in comparison with **S_4Cu**. It is likely that these solid-state structures are brought about as a consequence of combined influences of the distortions imposed by a short strap and crystal packing forces. Overall, the solid-state structural features of the strapped diporphyrins are consistent with the solution structures calculated by the MM2 method.

Oxidation potentials: The one-electron oxidation potentials of **S_n** were examined by cyclic voltammetry in DMF. Further coupling reactivity of these *meso*–*meso*-linked diporphyrins at free *meso*-positions upon the one-electron oxidation conditions[11, 18] precluded a clear detection of the relevant

0947-6539/03/0901-0062 $ 20.00+.50/0 *Chem. Eur. J.* **2003**, *9*, No. 1

Table 3. Structural parameters of X-ray crystal structures.

Compound	θ_S	θ_{NS}	δ_S	δ_{NS}	ϕ	χ	α	β	Cu – Cu[c]
2Cu[a]	86	89	64, 81	–	0.050	1.500	0.4	0.5, 0.7	8.338
S_8Cu[a]	65	80	66, 83	62, 69	0.328, 0.350	1.504	0.5, 0.6	3.4, 6.7	8.402
S_4Cu[a] (A)	61	68	52, 53	65, 75	0.645, 0.717	1.525	1.0, 2.0	3.0, 5.8	8.378
S_4Cu[a] (B)	53	59	58, 58	55, 78	0.604, 0.699	1.474	1.0, 2.2	4.2, 4.2	8.415
S_2Cu[b] (A)	51	59	47, 52	55, 72	0.464, 1.297	1.516	1.6, 4.2	1.4, 9.6	8.266
S_2Cu[b] (B)	50	55	48, 68	59, 76	0.152, 1.640	1.491	3.5, 4.0	3.5, 4.0	8.251

[a] At room temperature in capillary. [b] At 123 K. [c] Distance between two Cu atoms [Å].

Table 4. Crystal data and structure refinement of **2Cu**, **S_8Cu**, **S_4Cu**, and **S_2Cu**.

	2Cu	**S_8Cu**	**S_4Cu**	**S_2Cu**
formula	$C_{96}H_{102}N_8Cu_2 \cdot 2C_2H_6O \cdot 3H_2O$	$C_{88}H_{84}N_8O_2Cu_2 \cdot 5C_6H_6$	$C_{84}H_{75}N_8O_2Cu_2 \cdot 0.5CH_2Cl_2 \cdot CH_4O \cdot H_2O$	$C_{82}H_{72}N_8O_2Cu_2 \cdot 3C_7H_8$
M_r	1653.26	1803.34	1448.18	1605.04
T [K]	296	296	296	123
crystal system	monoclinic	triclinic	triclinic	triclinic
space group	*C*2/*c*	$P\bar{1}$	$P\bar{1}$	$P\bar{1}$
a [Å]	33.181(2)	18.396(2)	20.2162(2)	12.1232(1)
b [Å]	17.673(1)	18.895(2)	25.7703(6)	20.0051(6)
c [Å]	18.300(2)	18.145(1)	18.5239(2)	35.2829(3)
α [°]	90	117.298(4)	104.035(2)	91.975(3)
β [°]	116.849(2)	108.585(6)	95.242(1)	94.9120(1)
γ [°]	90	98.164(8)	107.654(3)	97.415(3)
V [Å]	9574.0(1)	4992(1)	8778.4(3)	8445.3(2)
Z	4	2	4	4
ρ_{calcd} [g cm^3]	1.141	1.200	1.096	1.262
μ [cm^{-1}]	4.97	4.81	5.63	5.60
F(000)	3480.00	1904.00	3032.00	3376.00
crystal size [mm^3]	0.60 × 0.40 × 0.40	0.40 × 0.15 × 0.10	1.0 × 0.30 × 0.20	0.60 × 0.20 × 0.10
$2\theta_{max}$ [°]	55.0	54.9	55.0	55.0
observed reflections	5086	6848	10296	12789
total reflections	11151	20199	32495	23091
parameters	422	1004	1513	1774
absorpn correction			empirical	
R_1 [$I > 3\sigma(I)$]	0.095	0.098	0.128	0.097
wR_2 [$I > 3\sigma(I)$]	0.112	0.116	0.165	0.119
GOF	5.420	0.660	1.000	0.750

oxidation potentials. However the one-electron oxidation potentials have been recorded by using the differential pulse voltammetry method and the results are summarized in Table 5. The one-electron oxidation potentials of **S_n** become gradually lower with a decrease in the strap length. To examine the dihedral angle dependence on the oxidation potentials in a clearer manner, we prepared *meso*-triaryl-substituted strapped diporphyrins **S'_8**, **S'_4**, and **S'_2** (see Scheme 1) that have no further coupling reactivity. The observed first (E_{ox1}) and second (E_{ox2}) oxidation potentials have been assigned as split first oxidation waves (one electron per porphyrin) judging from the data of other electronically coupled diporphyrins. The difference potential, $\Delta E = E_{ox2} - E_{ox1}$ increased upon decrease in the strap length, indicating that the effect of a hole at one Zn^{II} porphyrin for the neighboring Zn^{II} porphyrin increases in this order.

Table 5. Oxidation potentials in DMF [V; vs ferrocene/ferrocenium ion].

Compound	E_{ox1}	E_{ox2}	ΔE_{ox}[a]
1	0.33		
2	0.32		
S_{10}	0.33		
S_8	0.32		
S_6	0.31		
S_4	0.30		
S_3	0.28		
S_2	0.27		
S_1	0.22		
ZnTPP	0.37	–	–
2′	0.31	0.45	0.14
S'_8	0.31	0.45	0.14
S'_4	0.29	0.45	0.16
S'_2	0.26	0.43	0.17

[a] $\Delta E_{ox} = E_{ox2} - E_{ox1}$.

UV-visible absorption spectra: The electronic absorption spectra of **2** and **S_{10} – S_1** in CH_2Cl_2 are shown in Figure 6, and the numerical data are summarized in Table 6. The diporphyrin **S_{10}** exhibits split Soret bands at 414 and 447 nm, which are similar to those of **2**, except for a slight broadening. In going from **S_{10}** to **S_1**, the absorption spectra exhibit systematic changes both in the B- and Q-band regions. The intensities of the split Soret bands around 415 and 450 nm decrease and the absorption bands at ca. 400 and > 460 nm are intensified, particularly in **S_3**, **S_2**, and **S_1**. In the absorption spectrum of the most planar **S_1**, three distinct bands are observed at 395, 424, and 478 nm in the Soret band region. Along with these changes, the Q-bands display systematic changes including a change from a prominent Q(1,0)-band at

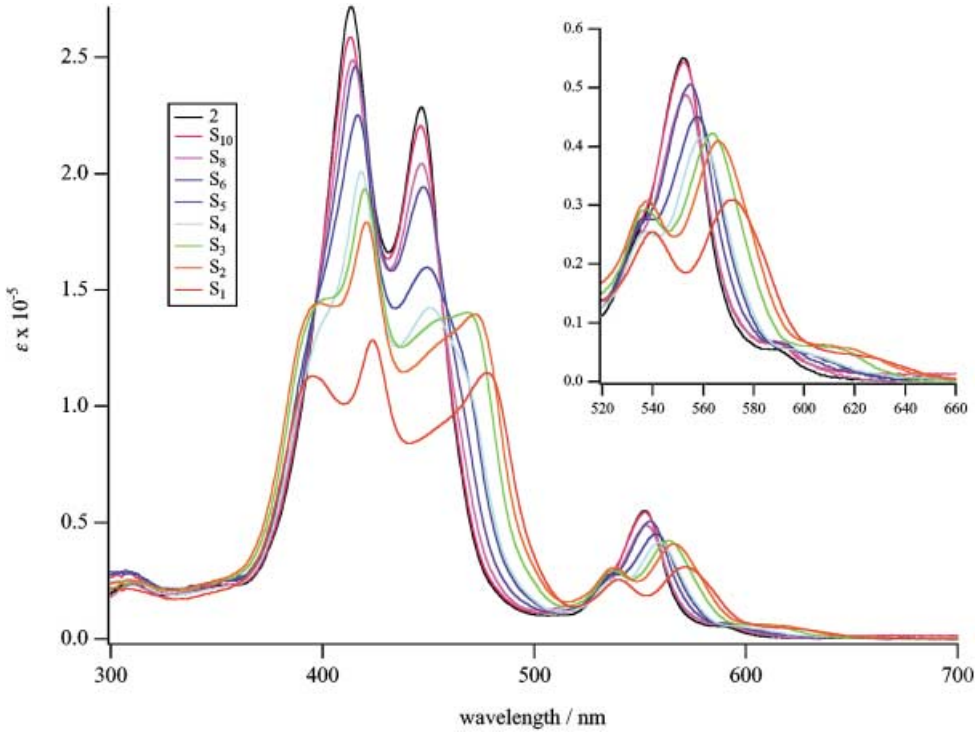

Figure 6. UV-visible absorption spectra of **2** and $\mathbf{S}_n$ in CH_2Cl_2.

Table 6. Data from absorption and CD spectra in CH_2Cl_2.

	Absorption spectra		CD spectra
	Soret λ_{max} ($\log\varepsilon$)	Q λ_{max} ($\log\varepsilon$)	λ_{max} ($\Delta\varepsilon$)
2[a]	414 (5.44), 447 (5.36)	552 (4.76), 589 (3.88)	399 (21.3), 417 (−39.8), 445 (9.3)
$\mathbf{S_{10}}$	414 (5.41), 447 (5.33)	553 (4.72), 589 (3.82)	398 (252.6), 416 (−933.2), 448 (134.0)
$\mathbf{S_8}$	415 (5.39), 447 (5.29)	554 (4.68), 591 (3.83)	398 (425.5), 417 (−1291.4), 448 (248.8)
$\mathbf{S_6}$	416 (5.39), 448 (5.29)	555 (4.70), 592 (3.81)	397 (502.5), 418 (−1841.6), 448 (274.2)
$\mathbf{S_5}$	417 (5.35), 450 (5.21)	538 (4.46), 559 (4.67), 595 (3.83)	394 (526.2), 419 (−1852.8), 453 (293.1)
$\mathbf{S_4}$	419 (5.30), 451 (5.16)	538 (4.44), 560 (4.64), 596 (3.74)	394 (555.5), 420 (−2211.4), 454 (312.4)
$\mathbf{S_3}$	420 (5.28), 469 (5.14)	538 (4.47), 564 (4.62), 611 (3.59)	392 (374.5), 422 (−1535.1), 466 (208.9)
$\mathbf{S_2}$	399 (5.18), 422 (5.25), 473 (5.16)	539 (4.53), 566 (4.61), 625 (3.66)	392 (243.2), 423 (−1066.1), 468 (142.1)
$\mathbf{S_1}$	395 (5.05), 424 (5.11), 478 (5.05)	540 (4.40), 572 (4.48), 625 (3.62)	392 (51.5), 425 (−224.8), 470 (39.0)

[a] CD data correspond to a nonstrapped chiral diporphyrin, see ref. [13].

552 nm and a weak Q(0,0)-band at 589 nm in $\mathbf{S_{10}}$ to distinct Q(2,0)- and Q(1,0)-bands at 540 and 572 nm, and a weak Q(0,0)-band at 625 nm in $\mathbf{S_1}$. It is noted here that there is a shoulder at the high-energy side of the Q(1,0)-band of **2** and $\mathbf{S_{10}}$, which is in the same position at 539 nm as the Q(1,0)-band of a monomer. Nearly at the same position, the Q(2,0)-band appears for all $\mathbf{S}_n$. Therefore it is conceivable that Q(2,0)-bands are insensitive to the change in the dihedral angle, whereas both Q(1,0)- and Q(0,0)-bands are sensitive to the dihedral angle and shift to the low-energy side upon a decrease in the strap length, thus enabling the observation of the distinct Q(2,0)-band in $\mathbf{S_3}-\mathbf{S_1}$.

Fluorescence spectra: The fluorescence spectra of **2** and $\mathbf{S}_n$ in CH_2Cl_2 are shown in Figure 7 and the numerical data are listed in Table 7. The nonstrapped diporphyrin **2** displays the fluorescence spectrum with a peak at 650 nm and a shoulder around 600 nm. As is the case for the absorption spectra, the strapped diporphyrin $\mathbf{S_{10}}$ exhibits a fluorescence spectrum that is similar to that of **2**. Along with the decrease in the strap length, the fluorescence spectra of $\mathbf{S}_n$ display systematic changes; namely, the fluorescence bands begin to merge into a single band and are shifted gradually to longer wavelength, roughly representing mirror images of the respective absorption Q(0,0)-bands. The fluorescence positions are almost the same in $\mathbf{S_{10}}-\mathbf{S_3}$, but those of $\mathbf{S_2}$ and $\mathbf{S_1}$ exhibit a distinct red-shift. The fluorescence quantum yields were determined in THF with reference to the value ($\Phi_F = 0.03$) reported for [Zn^{II}(tpp)] (tpp = 5,10,15,20-tetraphenylporphinate) in benzene.[19] Interestingly, the fluorescence quantum yield increases from $\mathbf{S_{10}}$ ($\Phi_F = 0.031$) to $\mathbf{S_3}$ ($\Phi_F = 0.051$) and decreases from $\mathbf{S_3}$ to $\mathbf{S_1}$ ($\Phi_F = 0.036$).

We also measured the emission spectra at 77 K in 2-methyltetrahydrofuran (MTHF) matrix (Supporting Information). Under these conditions, the fluorescence spectra of **2**, $\mathbf{S_{10}}$, $\mathbf{S_8}$, and $\mathbf{S_6}$ are similar in shape, featuring a small band around

0947-6539/03/0901-0064 $ 20.00+.50/0 *Chem. Eur. J.* **2003**, *9*, No. 1

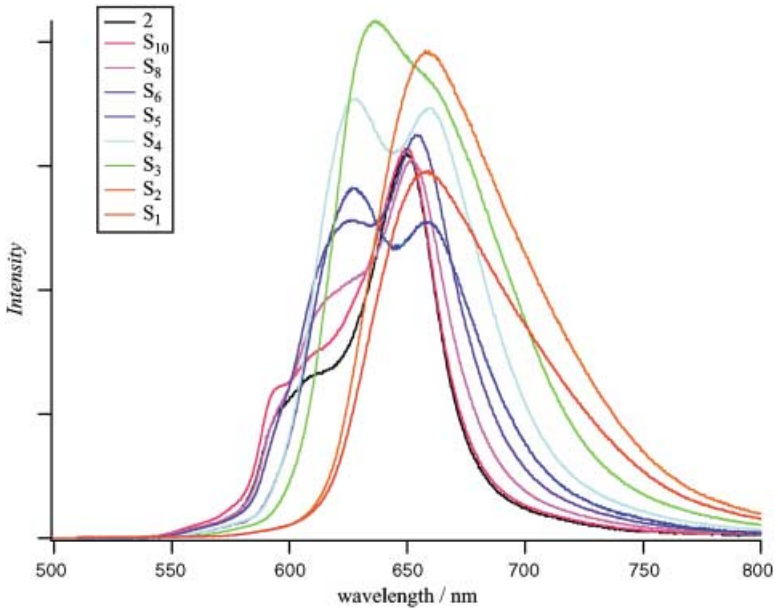

Figure 7. Fluorescence spectra of **2** and $\mathbf{S}_n$ in CH_2Cl_2.

Table 7. Data from fluorescence and phosphorescence spectra.[a]

	λ_F[b] (CH_2Cl_2)	Φ_F[c] (THF)	λ_F[b] (2-MTHF)	λ_F[d] (2-MTHF)	λ_P[d] (2-MTHF)
2	610,[e] 650	0.025	625,[e] 657	603, 662	771
$\mathbf{S_{10}}$	595,[e] 610,[e] 649	0.031	625,[e] 657	607, 660	767
$\mathbf{S_8}$	620,[e] 652	0.036	631, 659	610, 661	771
$\mathbf{S_6}$	626, 654	0.043	635, 658	609, 661	770
$\mathbf{S_5}$	626, 657	0.041	639	618, 671	775
$\mathbf{S_4}$	628, 659	0.051	641	622, 672	778
$\mathbf{S_3}$	637	0.055	651	637, 689	785
$\mathbf{S_2}$	658	0.045	657	642, 696	793
$\mathbf{S_1}$	658	0.036	666	652, 707	799

[a] Taken for excitation at the respective Soret bands (414–424 nm). [b] At room temperature. [c] Fluorescence quantum yield at room temperature. [d] At 77 K. [e] Shoulder.

603–620 nm and a large band around 660 nm, while the fluorescence spectra of $\mathbf{S_5}$, $\mathbf{S_4}$, $\mathbf{S_3}$, $\mathbf{S_2}$, and $\mathbf{S_1}$ exhibit large bands at 618–552 nm and small bands at 660–707 nm. Upon the decrease in the strap length, the relative intensity of the fluorescence band at lower energy side decreases and the fluorescence bands display a progressive red-shift in a systematic manner. At 77 K, the phosphorescence emissions from the lowest triplet excited state (T_1 state) are observed for all the strapped diporphyrins under the anaerobic conditions, and are also red-shifted upon the decrease in the strap length with less magnitude compared with a shift in the fluorescence (Table 7).

CD spectra: The strapped diporphyrins are chiral and have been all separated into the optically active enatiomers through a chiral HPLC column. The separated enantiomers are stable and do not racemize at room temperature.[16] The two isolated enantiomers display the opposite Cotton effects as shown for $\mathbf{S_{10}}$ in Figure 8. There is no significant Cotton effect in the Q-band region. The CD spectrum of the fast eluting isomer, $\mathbf{S_{10}}$(A) exhibited Cotton effects, positive at 446 nm, negative at 416 nm, and positive at 398 nm. We interpreted these CD spectra as a superposition of two bisignate split Cotton effects with opposite signs. In the case of $\mathbf{S_{10}}$(A), the first Cotton effect around 430 nm is positive and the second one around 405 nm is negative, and thus the negative band at 416 nm has the largest intensity. Figure 8 also show selected CD spectra of $\mathbf{S_4}$(A) and $\mathbf{S_1}$(A) (the CD spectra for all compounds are given in the Supporting Information; the numerical data are listed in Table 6). As the strap length is shortened, the first bisignate Cotton effect is red-shifted, while the second one remains at the nearly same position. The CD intensities also change with the strap length, curiously the largest for $\mathbf{S_4}$ in every band. These CD spectra provide important information on the absorption properties of the strapped diporphyrins, which will be discussed below.

Resonance Raman spectra: The resonance Raman (RR) spectra of $\mathbf{S}_n$'s ($n = 1, 2, 3, 4, 8$ and 10) and **2** are shown in Figure 9. The 457.9 and 488.0 nm Ar^+ ion laser lines

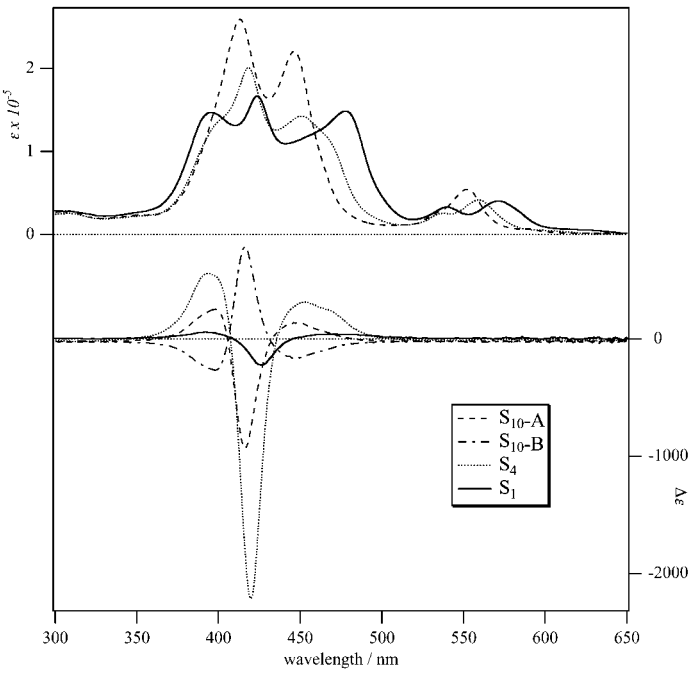

Figure 8. Absorption (upper) and CD spectra (bottom) of **2′**(A), $\mathbf{S_{10}}$(A), $\mathbf{S_{10}}$(B), $\mathbf{S_4}$(A), and $\mathbf{S_2}$(A) in CH_2Cl_2.

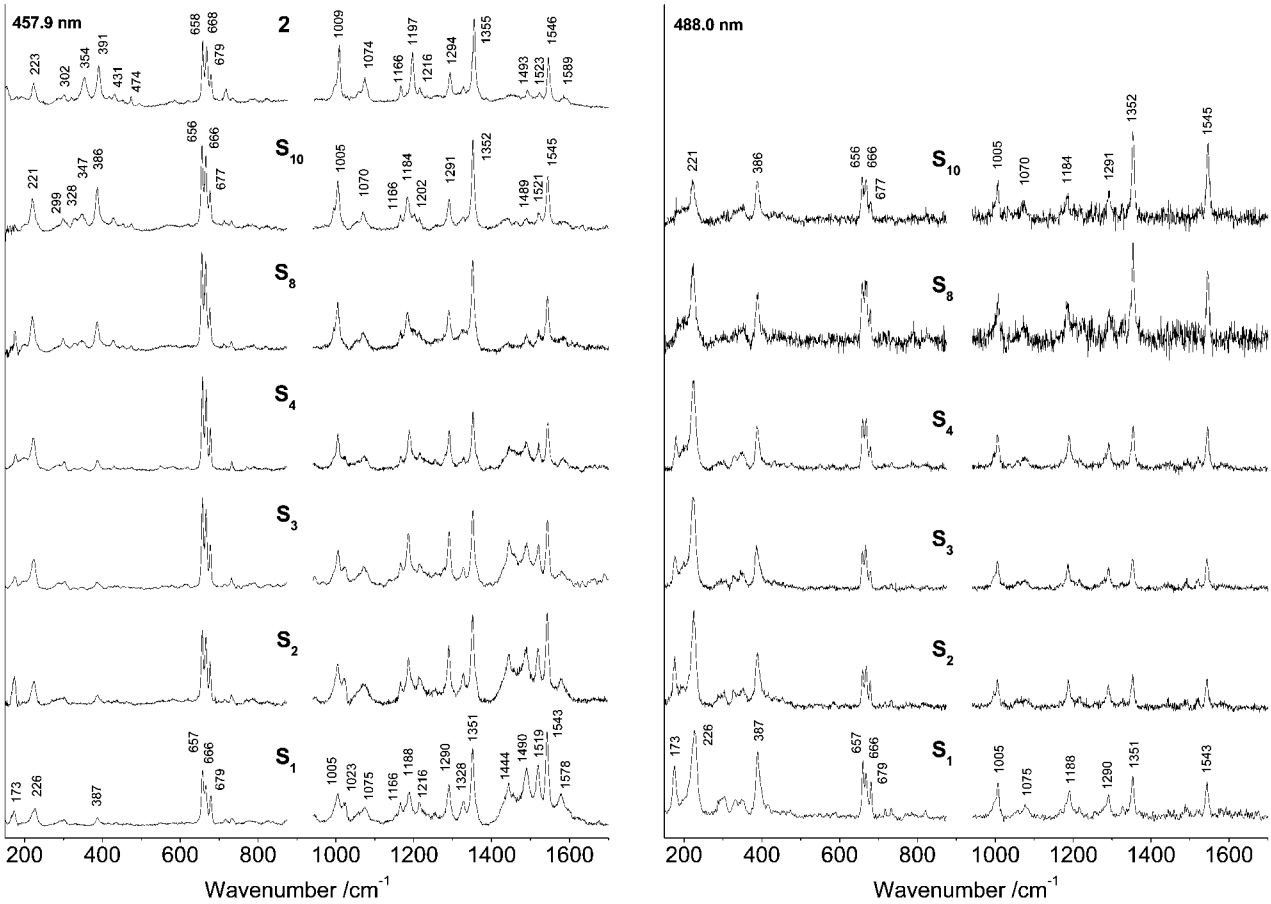

Figure 9. Resonance Raman spectra of $\mathbf{S}_n$ and **2** in THF with 457.9 nm excitation (left column), and those of $\mathbf{S}_n$ with 488.0 nm excitation (right column). The Raman bands from THF solvent were subtracted.

were selected as Raman excitation lines in order to elucidate charge transfer and excitonic nature of the absorption bands in 430–500 nm region. The RR spectrum of $\mathbf{S_{10}}$ by photoexcitation with the 457.9 nm laser line is similar to that of **2**, exhibiting the dominant enhancement of the Raman bands at 1545, 1352, 1291, 1184, 1070, 1005, 384, and 221 cm^{-1} and the triple bands at around 666 cm^{-1}. They all correspond to the totally symmetric A_1 modes under the D_{2d} symmetry point group of the orthogonal porphyrin dimer **2**. The Raman bands at 1545, 1352, 1070, 1005, and 386 cm^{-1} in the RR spectrum of $\mathbf{S_{10}}$ correspond to the ν_2, ν_4, ν_9, ν_6, and ν_8 modes of the porphyrin monomer; these are the totally symmetric A_{1g} modes.[20] The Raman bands at 1291, 1184, and 221 cm^{-1} correspond to the ν_{27}, ν_{51}, and ν_{35} modes of the porphyrin monomer. In going from $\mathbf{S_{10}}$ to $\mathbf{S_1}$, however, the Raman enhancement pattern shows the following systematic changes. The Raman bands at 1023, 1440, 1490, and 1519 cm^{-1} become gradually stronger and the low-frequency bands such as the ν_8 mode at about 387 cm^{-1} lose their intensities. The RR spectra of $\mathbf{S}_n$'s by photoexcitation with the 488.0 nm laser line reveal different features from those by photoexcitation with the 457.9 nm laser line, in that they all show nearly the identical enhancement pattern of the RR modes, except for a large enhancement of the low-frequency modes below 500 cm^{-1} with the decrease of the strap length. Most prominent Raman bands are the totally symmetric modes spanning the A_1 symmetry under the D_{2d} point group of the orthogonal porphyrin dimer **2**, as for the RR spectrum of $\mathbf{S_{10}}$ by photoexcitation with the 457.9 nm laser line.

A slight shift in vibrational frequency is observed for some Raman bands such as the ν_2 and ν_{35} modes. The ν_2 mode intrinsically involves the phenyl in-plane vibrational mode in the porphyrin monomer,[20a] and the ν_{35} mode involves the C_m phenyl motions in the orthogonal porphyrin dimer **2**.[20b] These frequency shifts are considered as reflecting the structural tension, especially in phenyl linkage strapping two porphyrins, enforced by the shortened strap length in going from $\mathbf{S_{10}}$ to $\mathbf{S_1}$ as indicated from the MM2 calculations and X-ray structures. The RR enhancement of the low-frequency modes below 400 cm^{-1} in going from $\mathbf{S_{10}}$ to $\mathbf{S_1}$ is worth noting. Previously we observed the similar RR enhancement in the low-frequency region by resonance excitation at the low-energy excitonic Soret band as the length of the orthogonal porphyrin arrays increased.[20b] This feature along with the invariant RR enhancement pattern from $\mathbf{S_{10}}$ to $\mathbf{S_1}$ by the 488.0 nm laser line excitation allows us to assign the 478 nm absorption band of $\mathbf{S_1}$ as the excitonic band. To understand the RR spectral changes by the 457.9 nm laser line excitation, we need to consider several aspects. The low-energy Soret band of $\mathbf{S_{10}}$ at 447 nm appears to shift to red up to 479 nm as the strap length becomes short, but a careful look of the absorption bands for $\mathbf{S_4}$ reveals clearly two bands slightly

0947-6539/03/0901-0066 $ 20.00+.50/0 *Chem. Eur. J.* **2003**, *9*, No. 1

overlapping with each other. Thus, even if the oscillator strength is small, it is regarded that the higher energy band still remains at around 450 nm and the lower energy band is shifted to red with gaining intensity. As previously noted, a slight charge-transfer character of the low-energy Soret band of **2** was revealed by the electronic absorption spectrum,[21] the absorption band at around 450 nm is attributed to the charge-transfer band, since the red-shifted absorption band at around 480 nm has strong excitonic nature. Thus, the RR bands that are enhanced only by the 457.9 nm laser line excitation are believed to arise from the charge-transfer character. The following theoretical study predicts the existence of the charge-transfer band (CT_y) and the excitonic band (B_x) in the spectral region from 450 to 480 nm, in which the former is less sensitive to the dihedral angle and the latter is much more sensitive.

Discussion

Although many strapped porphyrins have been prepared, our strategy is unique, in that the electronic coupling of porphyrins in *meso*–*meso*-coupled diporphyrins has been tuned by introducing a strap of varying length between the *meta*-positions of the 5-*meso*-aryl substituents, yet still keeping the center-to-center distance of the diporphyrins nearly constant. In the *meso*–*meso*-linked Zn^{II}-diporphyrins, it is anticipated that the electronic interactions between the porphyrins should be a minimum at the strict perpendicular conformation and can be enhanced upon tilting a dihedral angle from 90°. It is also anticipated that the electronic coupling should be larger in the S_2 state than in the S_1 state, since the transition dipole moments involved have larger oscillator strength in the former excited state.

The Ag^I-promoted coupling reaction has been demonstrated quite effective for the preparation of the strapped *meso*–*meso*-coupled diporphyrins with variable dihedral angles. It is worthwhile to note that considerably distorted strapped diporphyrins such as $\mathbf{S_3}$ and $\mathbf{S_2}$ with short straps have been successfully prepared by this coupling reaction; the even more distorted strapped diprphyrin $\mathbf{S_1}$, which has been shown to be thermally unstable and gradually decomposes, can be also prepared by this reaction.

As suggested from MM2 calculations and also from more elaborated calculation with B3LYP hybrid density-functional theory, nonstrapped *meso*–*meso*-linked diporphyrins like **2** seem conformationally rather flexible at a dihedral angle near 90°. Such a conformational flexibility may be common for the *meso*–*meso*-linked diporphyrins strapped by a longer chain, but not for those strapped by a shorter chain. In addition, the introduction of a short strap causes the deformation of a porphyrin ring; this complicates the system, since it would be very difficult to consider these two effects separately. The structural deformation accompanied by a decrease in the strap length has been also noted in the X-ray crystal structures. Structural distortions have been known to alter the optical and electrochemical properties of porphyrins.[22] However, as noted above, the observation that the *meso*-proton and the peripheral β-protons appear at almost the same chemical shifts in their ^{1}H NMR spectra indicates that a porphyrin ring current is not seriously affected by the deformations induced by this structural perturbation. Therefore, regardless of the conformational flexibility and the resultant structural deformation, which are variable for each *meso*–*meso*-linked strapped diporphyrin, it may be justified to discuss the systematic changes of the absorption spectra in terms of the averaged dihedral angle. This assumption has been supported by the facts that the ^{1}H NMR data and the crystal structures of the corresponding Cu^{II} complexes show a systematic decrease in the dihedral angle, reflecting a decrease in the strap length, roughly in line with the MM2 calculations

As shown in Figure 6, the strapped diporphyrins $\mathbf{S_{10}}$–$\mathbf{S_1}$ exhibit systematic changes in the electronic absorption spectra. In the first instance, we have attempted to explain these spectral changes in terms of the exciton coupling theory, in which the molecular orbitals of the porphyrin are localized on each porphyrin and the spectral changes are induced only by the Coulombic interactions of the relevant transition dipole moments. The absorption spectrum of **2** may be explained by considering Figure 10a, in which the transition dipole moments, $\boldsymbol{m}_{\perp\mathbf{1}}$, $\boldsymbol{m}_{\parallel\mathbf{1}}$, $\boldsymbol{m}_{\perp\mathbf{2}}$, and $\boldsymbol{m}_{\parallel\mathbf{2}}$, are placed in a perpendicular conformation of the diporphyrin. The interaction of $\boldsymbol{m}_{\perp\mathbf{1}}$ and $\boldsymbol{m}_{\perp\mathbf{2}}$ should be zero, leaving the absorption band at the same position of the Soret band of the porphyrin monomer, while the interaction of $\boldsymbol{m}_{\mathbf{1}}$ and $\boldsymbol{m}_{\parallel\mathbf{2}}$ should lead to dipole-allowed $\boldsymbol{m}_{\parallel\mathbf{1}}+\boldsymbol{m}_{\parallel\mathbf{2}}$ transition and dipole-forbidden $\boldsymbol{m}_{\parallel\mathbf{1}}-\boldsymbol{m}_{\parallel\mathbf{2}}$ transition, thus giving rise to a red-shifted Soret transition. This consideration can explain successfully the absorption spectra of a series of higher *meso*–*meso*-linked porphyrins.[11, 12a] In the case of a dihedral angle less than 90° (Figure 9b), the exciton coupling of $\boldsymbol{m}_{\perp\mathbf{1}}$ and $\boldsymbol{m}_{\perp\mathbf{2}}$ should be non-zero, making both $\boldsymbol{m}_{\perp\mathbf{1}}+\boldsymbol{m}_{\perp\mathbf{2}}$ and $\boldsymbol{m}_{\perp\mathbf{1}}-\boldsymbol{m}_{\perp\mathbf{2}}$ transitions dipole-allowed. The simple calculation predicts that $\boldsymbol{m}_{\perp\mathbf{1}}+\boldsymbol{m}_{\perp\mathbf{2}}$ transition should be higher in energy than $\boldsymbol{m}_{\perp\mathbf{1}}-\boldsymbol{m}_{\perp\mathbf{2}}$ transition by $2|\boldsymbol{m}_{\perp\mathbf{1}}||\boldsymbol{m}_{\perp\mathbf{2}}|\cos\theta/R^3$ (R is the center-to-center distance) and that the oscillator strength of the former should be larger than that of the latter. This seems to explain the splitting of the high-energy Soret band to two intense bands, for instance in the case of $\mathbf{S_1}$ at 395 and 424 nm, but their actual relative band intensities are opposite to that of the above simple prediction. More seriously, in the exciton coupling framework, the dipole-allowed $\boldsymbol{m}_{\parallel\mathbf{1}}+\boldsymbol{m}_{\parallel\mathbf{2}}$ transition should appear at the same position for all the strapped diporohyrins, since the Coulombic interaction between $\boldsymbol{m}_{\parallel\mathbf{1}}+\boldsymbol{m}_{\parallel\mathbf{2}}$ should be independent of the dihedral angle. This is not the case, since the intensity of the original red-shifted Soret band is decreased and the lowest Soret band is progressively shifted to the low-energy side upon the decrease in the strap length.

The CD spectra of the strapped diporphyrins suggest the presence of two Cotton effects. One is around at 400 nm and the other is around 420–440 nm. The Cotton effects at 400 nm can be assigned to the coupling of $\boldsymbol{m}_{\perp\mathbf{1}}$ and $\boldsymbol{m}_{\perp\mathbf{2}}$, since the two transition dipole moments are held in a chiral oblique geometry. As described above, the amplitudes of the Cotton effects are intensified from $\mathbf{S_{10}}$ to $\mathbf{S_4}$, and then attenuated from $\mathbf{S_4}$ to $\mathbf{S_1}$. The present systematic dependence of the observable $\Delta\varepsilon_{max}$ upon the dihedral angle (θ) seems to be consistent with

  0947-6539/03/0901-0067 $ 20.00+.50/0

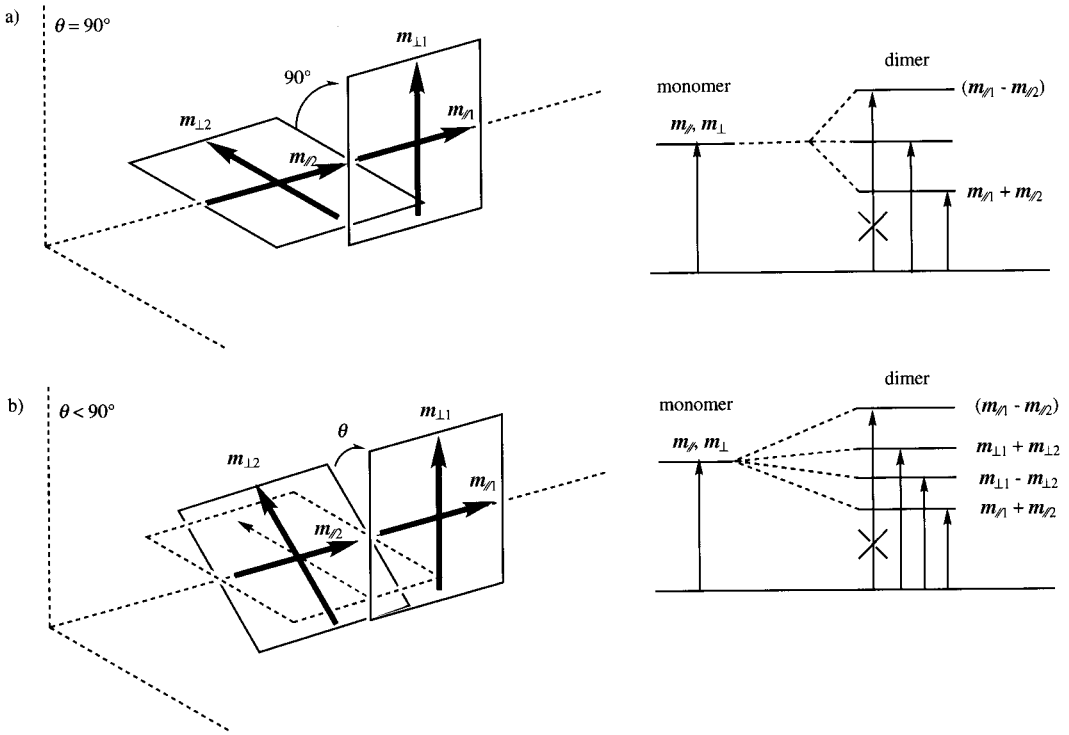

Figure 10. Schematic representations of the transition dipole moments of a) orthogonal diporphyrin and b) oblique diporphyrin.

simple calculation reported by Mason et al., in which the observable $\Delta\varepsilon_{max}$ of 9,9′-bianthryl derivatives was predicted to be the largest at about $\theta = 65-70°$.[23] On the other hand, the explanation of the Cotton effects at 420–440 nm is not straightforward within the framework of the exciton coupling, which does not include any intersubunit transition. One possibility is the coupling of $\boldsymbol{m}_{\|1}$ and $\boldsymbol{m}_{\|2}$ in a bent arrangement, which may be assessed by the parameter α. This can explain the opposite signs of the Cotton effects for the high- and low-energy sides. The bending is indeed true as judged from the determined X-ray crystal structures of $\mathbf{S_8}$, $\mathbf{S_4}$, and $\mathbf{S_2}$. However, $\boldsymbol{m}_{\|1}$ and $\boldsymbol{m}_{\|2}$ are arranged nearly in a linear fashion with small α values, which is quite unfavorable for the Cotton effects. Therefore, the observed comparable intensities of the two Cotton effects are difficult to explain solely by invoking the exciton coupling theory. Another possibility may be the presence of optical transitions over two porphyrin orbitals (intersubunit transitions), such as charge-transfer (CT) transitions, in this region. This consideration is likely to be consistent with the recent results on the electronic absorption spectra of *meso*–*meso*-linked diporphyrin doped in a PMMA polymer film; this indicates that there is a substantial change in electric dipole moment upon the transition at the split, lower energy Soret band.[21]

Molecular orbital (MO) considerations: To understand the absorption spectra of the strapped diporphyrins, we started with a simple quantum chemistry consideration[24, 25] and proceeded to more sophisticated calculations as described in the following. Initially, the strapped diporphyrins are modeled as a dimer of a simple unsubstituted porphin subunit with a variable dihedral angle (θ) between the *meso*–*meso* linkage as schematically displayed in Figure 10. All the geometries were optimized by using the B3LYP hybrid density-functional theory as implemented in the Gaussian 98 suite of programs;[26] the use of more convenient Hartree–Fock theory is not acceptable, since it is known to artificially favor a bond-alternating geometry for porphyrins.[27] The basis set used was the 6-31G[28] set for carbon, nitrogen, and hydrogen atoms, and Huzinaga's (14s8p5d) set contracted to [5s3p2d] for Zn.[29] The structures of the monomer and orthogonal diporphyrin were fully optimized under D_{4h} and D_{2d} symmetrical constraints, respectively, and have been calculated to gain the minimum-energy structures by performing the normal vibrational-mode analysis. For the diporphyrins that have θ less than 90°, all the geometrical parameters except θ were optimized assuming D_2 symmetry. As shown in Figure 11, the energy minimum is rather shallow around 90°, but the B3LYP total energy starts to increase significantly at around $\theta = 60°$ probably due to the increasing steric repulsion between the peripheral β-hydrogens adjacent to the *meso*–*meso* linkage. It is noteworthy that this repulsion also induces significant distortion in the porphyrin planes as displayed in Figure 11.

The absorption spectra of the model diporphyrins have been calculated by the single excited configuration interaction (SCI) method on the basis of the intermediate neglect of differential overlap model for spectroscopy (INDO/S) Hamiltonian.[30] The two-center Coulomb interactions were evaluated by the Nishimoto–Mataga formula.[31] Note that all the one-electron levels are considered in the SCI expansion taking advantage of the molecular D_2 symmetry to reduce the size of the Hamiltonian matrix. The Cartesian coordinate system in the SCI calculation is defined as shown in Figure 11,

0947-6539/03/0901-0068 $ 20.00+.50/0 *Chem. Eur. J.* **2003**, *9*, No. 1

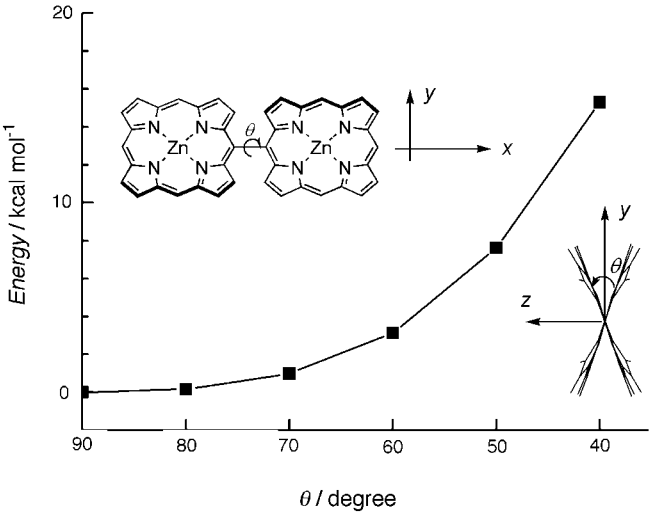

Figure 11. B3LYP-calculated torsional potential energy for the unsubstituted diporphyrin. The molecular structure is schematically represented in the top corner with the axis indication. The optimized structure ($\theta = 40^\circ$) is shown in the bottom corner.

in which the x, y, and z axes are set to coincide with the C_2 axes of the D_2 point group. On the basis of SCI excited states, the linear absorption spectrum Im$\alpha(\omega)$ was calculated by the standard sum-over-states formula[32] assuming a lifetime broadening of 0.1 eV for all the excited states.

The excited states of the diporphyrins have been characterized by utilizing the atomic-orbital (AO) representation of the transition density matrix [Eq. (1)]:[33]

$$\rho_{rs} = \langle e \,|\, a_r^\dagger a_s \,|\, g \rangle \tag{1}$$

in which $a_r^\dagger$ creates an electron at the rth AO, e represents the SCI excited state, and g is the Hartree–Fock ground state. The probability of simultaneously finding an electron at r and a hole at s is represented by $P_{rs} = \rho_{rs}^2/2$, in which the orthonormalization of AOs are assumed in the present scheme ensures $\sum_{r,s} P_{rs} = 1$ We define the interunit charge-transfer probability by Equation (2) in which $I(J)$ represents one porphyrin subunit in a dimer.

$$P_{CT} \equiv \sum_{I \neq J} \sum_{r \in I} \sum_{s \in J} P_{rs} \tag{2}$$

One-electron structure: The energy levels of the frontier eight orbitals (the highest four occupied and the lowest four unoccupied) for the diporphyrins obtained from INDO/S calculations are depicted in Figure 12 and the molecular orbitals (MOs) for the case of $\theta = 60^\circ$ are displayed in Figure 13. As can be seen, these eight orbitals are formed by combinations of monomer's four frontier orbitals,[34] which are also shown in Figure 13. A decrease in θ leads to a splitting of the degenerate e levels into the b_3 and b_2 levels along with their bonding and anti-bonding nature with respect to the π–π conjugation at the *meso*–*meso* linkage. It is to be noted here that the a_1 and b_1 levels are split even at $\theta = 90^\circ$, while their θ dependence is less significant than that for the b_2 and the b_3 levels; the *meso*–*meso* conjugation does not affect their

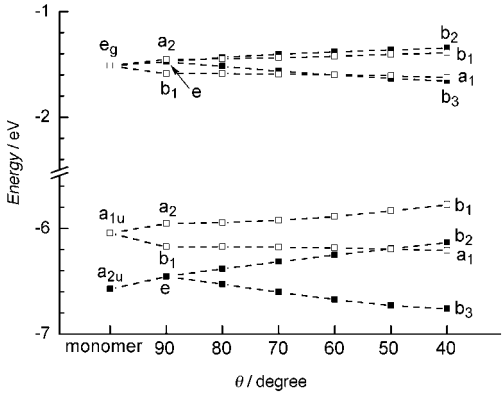

Figure 12. INDO/S-calculated energy level of the frontier eight orbitals versus inter-ring torsional angle of unsubstituted diporphyrin. The symmetry notation is that of D_{4h} for monomer and D_{2d} (D_2) for orthogonal (nonorthogonal) dimer.

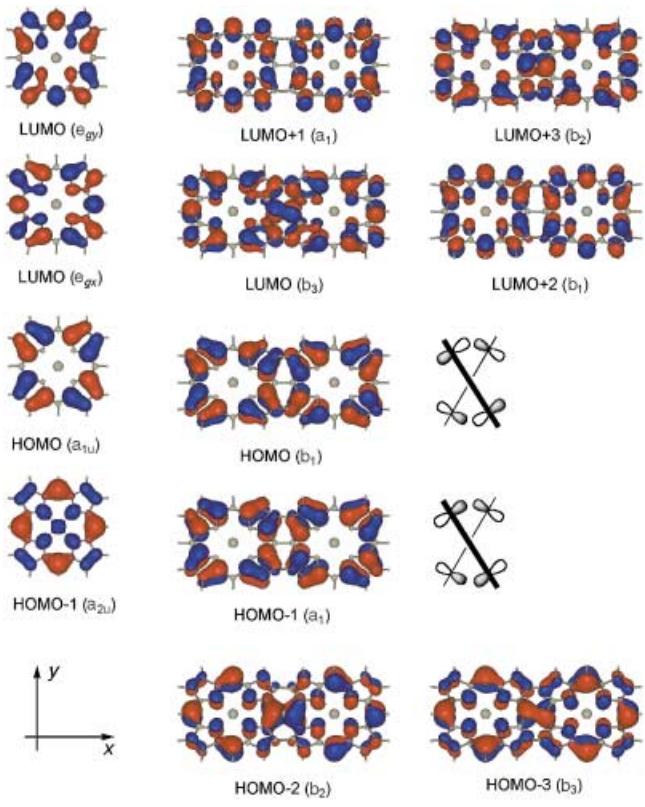

Figure 13. Frontier orbitals in monomer and dimer ($\theta = 60^\circ$). The situation of π–π overlap between α- or β-carbons in the adjacent porphyrin units are schematically shown for HOMO-1 (in-phase) and HOMO (out-of-phase).

energy levels, since the a_1 and b_1 MOs have nodes on the connecting *meso*-carbons. The splitting of the a_1 and b_1 levels can be explained in terms of through-space weak π-electron delocalization mediated by the non-zero overlap between π-atomic orbitals on either the α- or β-carbons of the adjacent porphyrin units (Figure 13); this kind of π interaction can be regarded as in-phase and out-of-phase combinations for the a_1 and b_1 levels, respectively, within a range of θ. For the b_2 and b_3 MOs, such interactions are canceled out at $\theta = 90^\circ$, whereas they compete with the electronic conjugation through the direct *meso*–*meso* connection at $\theta < 90^\circ$. It is also noted that

the energy splitting between bonding and anti-bonding orbitals is larger in the occupied space than in the unoccupied space.

Orthogonal diporphyrins: The calculated transition properties for the lowest 16 excited states of the orthogonal diporphyrin are listed in Table 8 together with their characteristics in terms of intersubunit charge-transfer probability (P_{CT}) calculated by Equation (2). The states arising from monomer's Q and B bands are designated by Q_i and B_i, respectively, where i ($=x, y, z$) stands for the orientation of the transition dipole moment as indicated by the present calculation ($i=0$ for a dipole-forbidden state). We note that the degenerate B_y and B_z are close in energy to the B band of a monomer, which was calculated to be 3.22 eV, and the B_x and B_0 are split into low- and high-energy sides, respectively. This situation is consistent with the exciton-coupling theory as evidenced by the essentially local excitation (LE) character of the B_i states as indicated by their P_{CT} values (Table 8). The relatively large CT contribution to the B_x band, which is caused by the above mentioned through-space, indirect π conjugation, would be responsible for the overestimation of the energy separation between the B_x and B_y (B_z) bands (calculated 0.32eV vs. observed 0.23 eV for $\mathbf{S_{10}}$). In this context, we point out a significant influence of *meso*-phenyl substituents on the electronic structure of excited states, since the energy separation has been calculated to be 0.28 eV for the *meso*-phenyl substituted diporphyrin.

Table 8. Transition properties and electronic structures of the lowest 16 singlet excited states of *meso*–*meso*-linked porphyrin dimers, as obtained from INDO/S-SCI calculations.

State	D_{2d}	D_2	ΔE [eV][a]	f[b]	P_{CT} [%][c]	W_8 [%][d]
$\theta=90^\circ$						
Q_x	B_2	B_1	1.81	0.102	2.1	96.7
Q_y	E	B_2	1.82	0.031	1.6	96.7
Q_z	E	B_3	1.82	0.031	1.6	96.7
Q_0	A_1	A_1	1.83	0	0.9	96.6
B_x	B_2	B_1	2.85	3.799	19.0	95.4
CT_y	E	B_2	2.87	0.087	92.3	93.8
CT_z	E	B_3	2.87	0.087	92.3	93.8
CT_0	A_1	A_1	3.01	0	99.1	98.5
CT_x	B_2	B_1	3.07	0.590	81.0	97.5
CT_x'	A_2	B_1	3.14	0	95.9	89.5
CT_0'	B_1	A_1	3.14	0	95.9	89.5
B_y	E	B_2	3.17	1.885	10.8	93.7
B_z	E	B_3	3.17	1.885	10.8	93.7
CT_y'	E	B_2	3.34	0.090	92.7	96.3
CT_z'	E	B_3	3.34	0.090	92.7	96.3
B_0	A_1	A_1	3.37	0	1.1	89.2
$\theta=60^\circ$						
Q_x		B_1	1.76	0.071	5.7	96.8
Q_y		B_2	1.77	0.045	6.1	96.8
Q_z		B_3	1.81	0.024	2.6	96.7
Q_0		A_1	1.83	0	2.2	96.5
B_x		B_1	2.70	3.631	33.0	94.4
CT_z		B_3	2.80	0.063	86.0	92.7
CT_y		B_2	2.82	0.266	84.3	93.4
CT_0		A_1	2.97	0	97.2	98.1
CT_x		B_1	3.03	0.119	89.9	97.0
B_z		B_3	3.05	0.812	26.1	93.0
CT_0'		A_1	3.09	0	86.2	89.4
B_y		B_2	3.12	1.706	42.6	94.3
CT_x'		B_1	3.33	0.792	64.7	89.9
CT_z'		B_3	3.36	0.173	74.7	92.8
B_0		A_1	3.39	0	7.6	88.0
CT_y'		B_2	3.46	0.768	42.7	68.0

[a] Excitation energy. [b] Oscillator strength. [c] Interunit charge-transfer probability [Eq. (2)]. [d] Total contribution of transitions within eight orbitals to the SCI wavefunction.

On the other hand, all the Q states have more clear LE character than the B states. The quite small ($\sim$0.01 eV) energy separation calculated for the Q_x and Q_y (Q_z) states leads to the assignment of the Q(0,0)-band (2.1 eV for $\mathbf{S_{10}}$) as a superposition of these transitions and supports the vibronic nature for the shoulder (Q(2,0)-band) observed on the high-energy side of the Q(1,0)-band.

In an energy range close to the B bands, we find eight charge-transfer (CT) states, which, together with the LE (Q_i and B_i) states, form a complete set of 16 eigenstates resulting from one-electron excitations within eight orbitals. As can be seen from their P_{CT} values, the mixing of LE and CT character in the excited states is minimized for the orthogonal diporphyrin due to nearly prohibited π-electron delocalization between the porphyrin subunits. For the description of these CT states, it is convenient to utilize the monomer's four orbitals localized in each subunit; these turn out to be basis functions for the C_{2v} subgroup of D_{2d} group. In terms of the transitions between these monomer MOs, the electronic wavefunctions of CT states (basis functions for both D_{2d} group and D_2 sub-group) are represented by Equations (3a) – (3d):

$$\Psi(CT_0,CT_x)=[\Phi(a_{1u}{}^L\rightarrow e_{gy}{}^R)\pm\Phi(a_{1u}{}^R\rightarrow e_{gy}{}^L)]/2^{1/2} \quad (3a)$$

$$\Psi(CT_y,CT_z)=[\Phi(a_{1u}{}^L\rightarrow e_{gx}{}^R)\pm\Phi(a_{1u}{}^R\rightarrow e_{gx}{}^L)]/2^{1/2} \quad (3b)$$

$$\Psi(CT_0', CT_x')=[\Phi(a_{2u}{}^L\rightarrow e_{gx}{}^R)\pm\Phi(a_{2u}{}^R\rightarrow e_{gx}{}^L)]/2^{1/2} \quad (3c)$$

$$\Psi(CT_y', CT_z')=[\Phi(a_{2u}{}^L\rightarrow e_{gy}{}^R)\pm\Phi(a_{2u}{}^R\rightarrow e_{gy}{}^L)]/2^{1/2} \quad (3d)$$

in which the superscripts L and R denote the left and right subunits, respectively, and the correspondence of ± combinations of Φ to the D_{2d} (D_2) representation listed in Table 8 depends on the signs of the basis MOs. Although the CT_x' state is dipole-forbidden in D_{2d} system, it becomes dipole-allowed by symmetry lowering to D_2 as θ deviates from 90°. It is noteworthy that for each direction of electron transfer (L → R or R → L), the above four configurations belong to different C_{2v} representations, which prohibit the configuration interaction among Ψs of Equations (3a) – (3d). The slight lifting of degeneracy for the CT_0-CT_x pair is due to the indirect π conjugation, while the degeneracy of the $CT_0'-CT_x'$ pair is retained under the π-electron approximation and lifted by the interaction with σ electrons.

The energy levels of the CT states should strongly depend on the intersubunit distance (the center-to-center distance of the two porphyrins), since the Coulomb attraction between electron and hole constitutes an important stabilizing factor.[24] In this regard, it is interesting to note that the energies of the CT_i and CT_i' states are roughly similar to those of the B_i states. This feature, which is quite specific to the *meso*–*meso*-linked diporphyrin, is caused by the situation that the two

0947-6539/03/0901-0070 $ 20.00+.50/0 *Chem. Eur. J.* **2003**, *9*, No. 1

porphyrins are located in a close proximity of the center-to-center distance of only 8.35 Å. In addition, the calculation has predicted that no CT state has sufficient oscillator strength to introduce any additional feature to the absorption spectrum of the orthogonal diporphyrin; this is dominated by the intense B_x and B_y (B_z) bands (Figure 14).

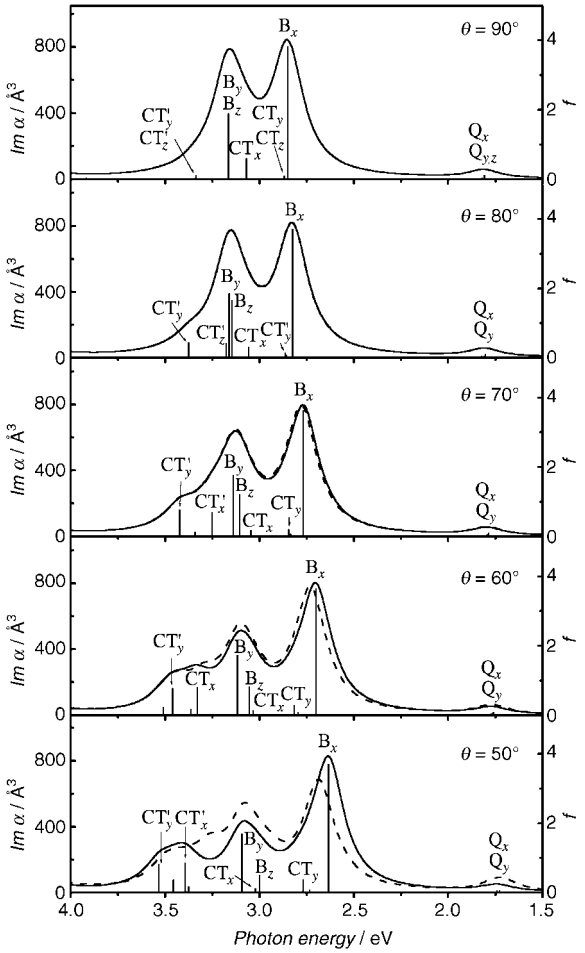

Figure 14. INDO/S-SCI simulated linear absorption spectra of diporphyrins on the basis of B3LYP optimized structures (solid curve); the vertical line indicates the oscillator strength (f) of each excited state. The spectra shown by dashed line are obtained for the dimers with undistorted porphyrin rings (i.e. the geometry optimized at $\theta = 90°$).

Not orthogonal diporphyrins: The INDO/S-SCI-simulated linear absorption spectra for the dimers of $\theta < 90°$ are displayed in Figure 14 (solid line) and the transition properties of the lowest 16 excited states for a diporphyrin with $\theta = 60°$ are listed in Table 8 (the notation of excited states, following that of the orthogonal diporphyrin, has been done on the basis of main contributions to their SCI expansions). In these calculated spectra, experimentally observed features mentioned above are well reproduced. To reveal the influence of ring distortion, we have also performed INDO/S-SCI calculations for the dimers composed of flat porphyrin subunits whose geometries are obtained by changing only θ in the optimized geometry of orthogonal dimer. The results are plotted by dotted lines in Figure 14. We note the spectral change is caused essentially by the dihedral angle, while the ring distortion enhances the red-shift of the B_x band and makes more clear the absorption on the high-energy side of the B_y band.

The symmetry lowering from D_{2d} to D_2 lifts the degeneracy of excited states. The splitting of the $B_y - B_z$ pair follows the exciton coupling scheme with the B_y carrying more intensity and lying at the high-energy side (Figure 14). However, their energy separation is so small (0.07 eV at $\theta = 60°$) that they would merge into a single band that probably corresponds to an intense peak around 420 nm in the $\mathbf{S_3}$, $\mathbf{S_2}$, and $\mathbf{S_1}$ spectra.

On the other hand, as shown in Figure 14, we find that the absorption appearing on the high-energy side of the B_y band (about 400 nm in the $\mathbf{S_3}$, $\mathbf{S_2}$, and $\mathbf{S_1}$ spectra) is formed by a superposition of the CT'_x and CT'_y transitions. As shown in Table 8, these states show remarkable enhancement in their oscillator strengths and the CT'_x is significantly blue-shifted at $\theta = 60°$ relative to the case of $\theta = 90°$. In this context, it is worthwhile to point out that the ring distortion enhances the blue-shift of the CT'_x; this may be responsible for the more pronounced peak calculated for the ring-distorted geometry (Figure 14).

In the energy region between the B_x and B_y bands, we note that the oscillator strength of the CT_y state is significantly enhanced, while that of the CT_x state is attenuated upon a decrease in the dihedral angle. In addition, the associated red-shifts of these CT states are less prominent relative to that of the B_x band. Therefore, the above-mentioned RR bands that are enhanced only by the 457.9 nm excitation are considered to arise from the CT_y state. The observed Cotton effects at longer wavelength can be similarly explained in terms of the CT_y state, which has been calculated to be slightly red-shifted upon a decrease in θ.

The above mentioned intensification of the CT_y, CT'_x, and CT'_y states can be ascribed to the enhanced LE character in their electronic structures (Table 8). Moreover, this situation can be regarded as a result of configuration mixing between these charge-transfer states and B_i ($i = x, y$) states caused by the increased *meso–meso* π conjugation, since the CT contribution is significantly enhanced in the latter.

In contrast to the case of $B_y - B_z$ pair, the calculation predicts that the Q_y shifts to the low-energy side of the Q_z as θ deviates from 90°. Then, the red-shifted Q(0,0)-band observed for $\mathbf{S_n}$ would be assigned to a superposition of the Q_x and the Q_y transitions. Note that, in contrast to the B states, all of the Q states retain their LE character, even for the twisted geometries. This would be due to their energy separation from the CT states that prohibits efficient configuration interactions among them.

This calculation has shown that the red-shifts of the Q_x (Q_y), B_x, and B_y bands, in going from $\theta = 90°$ to 60°, are 0.05 (0.05), 0.15, and 0.05 eV, respectively. These values are in a good agreement with the corresponding values of 0.12, 0.18, and 0.08 eV obtained from the $\mathbf{S_{10}}$ and $\mathbf{S_2}$ spectra ($\theta_S = 65°$ and $\theta_{NS} = 73°$ in the X-ray structure of $\mathbf{S_2}$).

The more significant red-shift of the B_x band relative to those for the Q_x, Q_y, and B_y bands can be explained on the basis of the one-electron structure of dimer (Figure 13) and the SCI expansion of each excited state (Table 9). For the B_x band, the contribution of $b_2 \rightarrow b_3$ transition increases, while

  0947-6539/03/0901-0071 $ 20.00+.50/0

Table 9. Dependence of the SCI expansion coefficients for the singlet excited states on the interunit torsion angle θ of the *meso*–*meso*-linked porphyrin dimers.

State	Transition	θ [°]				
		90	80	70	60	50
Q_x	ΔE[a]	1.81	1.80	1.79	1.76	1.73
	$b_1 \rightarrow a_1$	−0.63	−0.63	−0.63	−0.64	−0.65
	$a_1 \rightarrow b_1$	−0.47	−0.47	−0.45	−0.44	−0.41
	$b_2 \rightarrow b_3$	0.42	0.45	0.48	0.51	0.53
	$b_3 \rightarrow b_2$	0.42	0.38	0.35	0.33	0.30
Q_y	ΔE	1.82	1.81	1.79	1.77	1.74
	$b_1 \rightarrow b_3$	−0.60	−0.61	−0.63	−0.65	−0.67
	$a_1 \rightarrow b_2$	−0.49	−0.47	−0.44	−0.42	−0.39
	$b_2 \rightarrow a_1$	−0.45	−0.47	−0.49	−0.50	−0.51
	$b_3 \rightarrow b_1$	−0.41	−0.39	−0.37	−0.34	−0.32
B_x	ΔE	2.85	2.82	2.77	2.70	2.63
	$b_1 \rightarrow a_1$	0.64	0.62	0.59	0.58	0.59
	$a_1 \rightarrow b_1$	0.06	0.09	0.12	0.14	0.13
	$b_2 \rightarrow b_3$	0.52	0.68	0.74	0.76	0.76
	$b_3 \rightarrow b_2$	0.52	0.32	0.19	0.13	0.09
B_y	ΔE	3.17	3.16	3.14	3.12	3.09
	$b_1 \rightarrow b_3$	0.25	0.22	0.19	0.15	0.12
	$a_1 \rightarrow b_2$	0.58	0.57	0.58	0.61	0.64
	$b_2 \rightarrow a_1$	−0.64	−0.74	−0.76	−0.74	−0.71
	$b_3 \rightarrow b_1$	−0.35	−0.15	−0.02	0.05	0.09

[a] Excitation energy in eV.

that of $b_3 \rightarrow b_2$ decreases as θ deviates from 90°. This trend is consistent with the red-shift of the B_x band, since the one-electron transition energy for the former is lowered while that for the latter is raised. Although a similar situation is observed for the SCI expansion of the Q_x band, it is not so remarkable as the case of the B_x band. For the Q_y and B_y bands, the net increase in the overall contribution of energy-lowering transitions is much smaller than that for the B_x band.

On the basis of the present calculation, the low-energy Soret bands for **S_{10}**, **S_8**, and **S_6** (ca. 450 nm) and the 470–480 nm absorption bands for **S_2** and **S_1** are assigned to the B_x state, which is essentially of excitonic nature as revealed by the calculation. In addition, the calculation has predicted that the CT_y state is located just on the high-energy side of the B_x state, and the red-shift of the former is less significant relative to the latter. Then, the 450–460 nm absoption feature for **S_2** and **S_1** can be assigned to the CT_y state; the contribution of the CT_y should be negligible as compared with that of the intense B_x band for dimers with longer strap length. However, these assignments can not be applied to the two-band nature clearly observed for **S_4**, for which the high-energy component is more intense than the low-energy one in contradiction to the predicted relationship between the B_x and CT_y states. To explain this absorption feature, it might be required to take account of the actual structure of the strapped diporphyrin including the distribution of dihedral angle in solution.

As discussed above, the INDO/S-SCI calculation has been used to predict several CT transitions, some of which are accidentally located in energy close to the excitonic transitions, including the B_x, B_y, and B_z bands. This unique situation is evidently caused by the close proximity of the directly linked porphyrins. The INDO/S calculation has also predicted the significant contribution of several CT states (especially the CT'_x and CT'_y) to the spectral change caused by the shortening of the strap length in **S_n**. The simple exciton coupling theory is insufficient to explain even qualitatively the photophysical properties of **S_n**. In this respect, the INDO/S calculation is quite complementary, successfully addressing the unique photophysical properties of **S_n**.

Conclusion

A series of the *meso*–*meso*-linked strapped diporphyrins **S_n** with various strap lengths was effectively synthesized by the intramolecular Ag^I-promoted coupling of the bridged diporphyrins **B_n** in dilute conditions. It has been shown that the dihedral angles between the diporphyrins can be set in a predictable manner by introducing a strap of variable length and the electronic interactions between the two porphyrins are increased upon the decrease of the dihedral angle as revealed by the absorption, fluorescence, and CD spectra, and the one-electron oxidation potentials. Hence, this system offers a nice set of diporphyrins with variable electronic interactions and a constant center-to-center distance; this is promising for the energy- and electron-transfer studies, which are now actively in progress in our laboratory.

Experimental Section

All reagents or solvents were of the commercial reagent grade and were used without further purification except where noted. Dry CH_2Cl_2 and $CHCl_3$ were obtained by refluxing and distilling over CaH_2. ^1H NMR spectra were recorded in $CDCl_3$ on a JEOL ALPHA-500 spectrometer, and chemical shifts were represented as δ values in ppm relative to the internal standard of $CHCl_3$ (7.260 ppm). UV-visible absorption spectra were recorded on a Shimadzu UV-2400PC spectrometer. Steady-state fluorescence emission spectra were recorded on a Shimadzu RF-5300PC spectrometer. CD spectra were recorded on a JASCO J-720 spectrometer. Mass spectra were recorded on a JEOL HX-110 spectrometer, by using positive-FAB ionization method (accelerating voltage 10 kV) with a 3-nitrobenzylalcohol matrix. Redox potentials were measured by cyclic voltammetry or differential pulse voltammetry on a BAS electrochemical analyzer model 660. The ground-state RR spectra of the porphyrin arrays were obtained by photoexcitation using 457.9 and 488.0 nm lines from a continuous wave Ar ion laser (Coherent INNOVA 90). Raman scattering signals were collected in 90° scattering geometry and detected by a 1-m double monochromator (ISA Jobin-Yvon U-1000) equipped with a thermoelectrically cooled photomultiplier tube (Hamamatsu R943–02). The Raman spectra were recorded on a single pass spectrometer (ISA Jobin-Yvon HR640) with a gated intensified charge-coupled device (ICCD, Princeton Instruments IRY700) detector and a pulse generator (Princeton Instruments FG100). X-ray crystallography was performed on a Rigaku-Raxis imaging plate system ($\lambda = 0.7107$). Gel permeation chromatography (GPC) and high-pressure liquid chromatography (HPLC) was performed on JAIGEL 2.5HA, 3HA, and 4HA columns with a JASCO HPLC system by using multiwavelength detector MD-915. Separation of enantiomers was performed on an analytical Sumichiral OA4400 column with a Shimadzu HPLC system with a multiwavelength detector SPD-M10AVP. Preparative GPC was carried out on a gravity column filled with BioRad Bio-Beads SX-1. Preparative separations were performed by silica gel flash column chromatography (Merck Kieselgel 60H Art.7736) and silica gel gravity column chromatography (Wako gel C-200).

5-(3,5-Di-*tert*-butylphenyl)-15-(3-methoxyphenyl)porphyrin: A solution of dipyrromethane (458 mg, 3.1 mmol), 3,5-di-*tert*-butylbenzaldehyde (330 mg, 1.6 mmol), and *m*-anisaldehyde (1.6 mmol) in dry CH_2Cl_2 (600 mL) was stirred under with N_2 for 15 min. Trifluoroacetic acid

0947-6539/03/0901-0072 $ 20.00+.50/0 *Chem. Eur. J.* **2003**, *9*, No. 1

(0.15 mL, 2 mmol) was added to the solution by syringe, the flask was shielded from light, and the solution was stirred for 1 h at room temperature. *o*-Chloranil (0.98 g, 4 mmol) was added, and the solution was stirred for an additional 30 min. The mixture was directly passed through an alumina column and evaporated. Porphyrin products were separated by a silica gel chromatography with CH_2Cl_2/hexane (1:1) as an eluent. The target porphyrin product was obtained after recrystallization from CH_2Cl_2/methanol in 18% yield: ^{1}H NMR ($CDCl_3$): $\delta = 10.32$ (s, 2H), 9.41 (d, $J =$ 5 Hz, 2H) , 9.40 (d, $J = 5$ Hz, 2H), 9.15 (d, $J = 5$ Hz, 2H), 9.14 (d, $J = 5$ Hz, 2H), 8.16 (s, 2H), 7.90 (d, $J = 3$ Hz, 1H), 7.86 (s, 2H), 7.71 (t, $J = 8$ Hz, 1H), 7.38 (dd, $J = 3$, 9 Hz, 1H), 4.03 (s, 3H), 1.59 (s, 18H), -3.04 ppm (br d, 2H); FAB HRMS: *m*/*z* calcd for $C_{41}H_{40}N_4O$ 604.3202; found: 604.3289.

5-(3,5-Di-*tert*-butylphenyl)-15-(3-hydroxyphenyl)porphyrin (1): A solution of 5-(3,5-di-*tert*-butylphenyl)-15-(3-methoxyphenyl)porphyrin (300 mg, 0.50 mmol) in dry CH_2Cl_2 (60 mL) was cooled to 0° C under Ar. A solution of BBr_3 (2.0 mL, 7.6 mmol) in dry CH_2Cl_2 (10 mL) was added dropwise over 10 min. The mixture was allowed to warm slowly to room temperature and was stirred for 5 h, poured into water, and extracted with CH_2Cl_2; the combined organic extracts were washed successively with water, $NaHCO_3$ solution, and water, and dried over anhydrous Na_2SO_4 and evaporated. The product porphyrin was purified by silica gel column chromatography with $CHCl_3$ as an eluent. Compound **1** was obtained after recrystallization from CH_2Cl_2/hexane in 96% yield (285 mg): ^{1}H NMR ($CDCl_3$): $\delta = 10.30$ (s, 2H), 9.39 (d, $J = 4$ Hz, 2H), 9.37 (d, $J = 5$ Hz, 2H), 9.14 (d, $J = 4$ Hz, 2H), 9.10 (d, $J = 5$ Hz, 2H), 8.15 (d, $J = 2$ Hz, 2H), 7.86 (t, $J = 2$ Hz, 1H), 7.85 (d, $J = 7$ Hz, 1H), 7.68 (br s, 1H), 7.64 (t, $J = 8$ Hz, 1H), 7.27 (d, $J = 3$ Hz, 1H), 5.15 (br s, 1H), 1.59 (s, 18H), -3.07 ppm (br s, 2H); FAB HRMS: *m*/*z* calcd for $C_{40}H_{38}N_4O$ 590.3046; found: 590.3102,.

General procedure for the preparation of B_n: Anhydrous K_2CO_3 was stirred and heated under reduced pressure overnight and then cooled to room temperature under argon. A solution of **1** and dibromoalkane in dry acetone or dry DMF was then added. The resultant mixture was heated to reflux under argon for between 3 h and 2 d. The reaction mixture was poured into water and extracted with CH_2Cl_2. The combined extracts were washed with water, dried over Na_2SO_4, and evaporated. The product was purified by silica gel flash column chromatography with CH_2Cl_2/hexane (1:1) as an eluent. Zinc(II) metallation was quantitatively carried out by stirring a solution of diporphyrin in CH_2Cl_2 in the presence of $Zn(OAc)_2$.

Decamethylene-1,10-dioxy-bridged Zn^{II} diporphyrin B_{10}: Diporphyrin $\mathbf{B_{10}}$ was prepared from the reaction of **1** (145 mg, 0.24 mmol) and 1,10-dibromodecane (18 μL, 0.08 mmol) in dry acetone (20 mL) in the presence of anhydrous K_2CO_3 (277 mg, 2.0 mmol) in 86% yield (149 mg): ^{1}H NMR ($CDCl_3$): $\delta = 10.21$ (s, 4H), 9.40 (d, $J = 5$ Hz, 4H), 9.34 (d, $J = 5$ Hz, 4H), 9.22 (d, $J = 5$ Hz, 4H), 9.13 (d, $J = 5$ Hz, 4H), 8.18 (t, $J = 3$ Hz, 4H), 7.88 (t, $J = 2$ Hz, 2H), 7.79 (d, $J = 7$ Hz, 2H), 7.77 (s, 2H), 7.63 (t, $J = 8$ Hz, 2H), 7.28 (dd, $J = 3$, 8 Hz, 2H), 4.09 (t, $J = 7$ Hz, 4H), 1.84 (m, 4H), 1.61 and 1.60 (s, 18H), 1.47 (m, 4H), 1.34 (m, 4H), 0.92 ppm (m, 4H); FAB HRMS: *m*/*z* calcd for $C_{90}H_{90}N_8O_2Zn_2$: 1442.5770; found: 1442.5830; UV/Vis (CH_2Cl_2): $\lambda_{max} = 409$, 537, 570 nm; fluorescence (CH_2Cl_2, $\lambda_{ex} = 409$ nm): $\lambda_{em} = 576$, 628 nm.

Octamethylene-1,8-dioxy-bridged Zn^{II} diporphyrin B_8: Diporphyrin $\mathbf{B_8}$ was prepared from the reaction of **1** (120 mg, 0.20 mmol) and 1,8-dibromooctane (20 μL, 0.10 mmol) in dry acetone (20 mL) in the presence of anhydrous K_2CO_3 (277 mg, 2.0 mmol) in 82% yield (116 mg): ^{1}H NMR ($CDCl_3$): $\delta = 10.25$ (s, 4H), 9.41 (d, $J = 5$ Hz, 4H), 9.36 (d, $J = 4$ Hz, 4H), 9.19 (d, $J = 5$ Hz, 4H), 9.14 (d, $J = 5$ Hz, 4H), 8.14 (t, $J = 3$ Hz, 4H), 7.85 (t, $J = 2$ Hz, 2H), 7.82 (d, $J = 2$ Hz, 2H), 7.79 (d, $J = 7$ Hz, 2H), 7.62 (t, $J =$ 8 Hz, 2H), 7.30 (dd, $J = 3$, 8 Hz, 2H), 4.14 (t, $J = 7$ Hz, 4H), 1.88 (m, 4H), 1.6–1.5 (m, 8H), 1.58 (s, 18H), 1.57 ppm (s, 18H); FAB HRMS: *m*/*z* calcd for $C_{88}H_{86}N_8O_2Zn_2$: 1414.5457; found: 1414.5503; UV/Vis (CH_2Cl_2):$\lambda_{max} =$ 409, 534, 574 nm; fluorescence (CH_2Cl_2, $\lambda_{ex} = 409$ nm): $\lambda_{em} = 576$, 628 nm.

Hexamethylene-1,6-dioxy-bridged Zn^{II} diporphyrin B_6: Diporphyrin $\mathbf{B_6}$ was prepared from the reaction of **1** (122 mg, 0.20 mmol) and 1,6-dibromohexane (16 μL, 0.10 mmol) in dry acetone (20 mL) in the presence of anhydrous K_2CO_3 (280 mg, 2.0 mmol) in 83% yield (119 mg): ^{1}H NMR ($CDCl_3$): $\delta = 10.25$ (s, 4H), 9.41 (d, $J = 5$ Hz, 4H), 9.36 (d, $J = 4$ Hz, 4H), 9.19 (d, $J = 4$ Hz, 4H), 9.15 (d, $J = 5$ Hz, 4H), 8.14 (t, $J = 3$ Hz, 4H), 7.85 (s, 2H), 7.82 (s, 2H), 7.79 (d, $J = 8$ Hz, 2H), 7.62 (t, $J = 8$ Hz, 2H), 7.33 (dd, $J =$ 3, 8 Hz, 2H), 4.20 (t, $J = 7$ Hz, 4H), 1.96 (m, 4H), 1.67 (m, 4H), 1.57 ppm (s, 36H); FAB HRMS: *m*/*z* calcd for $C_{86}H_{82}N_8O_2Zn_2$: 1386.5144; found: 1386.5072; UV/Vis (CH_2Cl_2): $\lambda_{max} = 409$, 537, 572 nm; fluorescence (CH_2Cl_2, $\lambda_{ex} = 409$ nm): $\lambda_{em} = 578$, 627 nm.

Pentamethylene-1,5-dioxy-bridged Zn^{II} diporphyrin B_5: Diporphyrin $\mathbf{B_5}$ was prepared from the reaction of **1** (50 mg 85 μmol) and 1,5-dibromohexane (5.8 μL, 42 μmol) in dry acetone (5 mL) in the presence of anhydrous K_2CO_3 (120 mg, 0.87 mmol) in 70% yield (41 mg): ^{1}H NMR ($CDCl_3$): $\delta =$ 10.22 (s, 4H), 9.39 (d, $J = 5$ Hz, 4H), 9.34 (d, $J = 4$ Hz, 4H), 9.19 (d, $J =$ 5 Hz, 4H), 9.15 (d, $J = 5$ Hz, 4H), 8.14 (t, $J = 3$ Hz, 4H), 7.86 (s, 2H), 7.83 (s, 2H), 7.79 (d, $J = 8$ Hz, 2H), 7.63 (t, $J = 8$ Hz, 2H), 7.33 (dd, $J = 3$, 8 Hz, 2H), 4.23 (t, $J = 7$ Hz, 4H), 2.02 (m, 4H), 1.82 (m, 2H), 1.58 ppm (s, 36H); FAB HRMS: *m*/*z* calcd for $C_{86}H_{82}N_8O_2Zn_2$: 1372.4987; found: 1372.5109; UV/Vis (CH_2Cl_2): $\lambda_{max} = 408$, 537, 572 nm; fluorescence (CH_2Cl_2, $\lambda_{ex} = 408$ nm): $\lambda_{em} = 576$, 629 nm.

Tetramethylene-1,4-dioxy-bridged Zn^{II} diporphyrin B_4: Diporphyrin $\mathbf{B_4}$ was prepared from the reaction of **1** (140 mg, 0.24 mmol) and 1,4-dibromobutane (14 μL, 0.12mmol) in dry acetone (20 mL) in the presence of anhydrous K_2CO_3 (328 mg, 2.3mmol) in 92% yield (150 mg): ^{1}H NMR ($CDCl_3$): $\delta = 10.21$ (s, 4H), 9.38 (d, $J = 5$ Hz, 4H), 9.33 (d, $J = 5$ Hz, 4H), 9.18 (d, $J = 4$ Hz, 4H), 9.16 (d, $J = 4$ Hz, 4H), 8.14 (br s, 2H), 8.12 (br s, 2H), 7.87 (br s, 2H), 7.84 (br s, 2H), 7.82 (d, $J = 8$ Hz, 2H), 7.63 (t, $J = 8$ Hz, 2H), 7.36 (dd, $J = 2$, 8 Hz, 2H), 4.33 (br s, 4H), 2.19 (br s, 4H), 1.57 ppm (s, 36H); FAB HRMS: *m*/*z* calcd for $C_{84}H_{78}N_8O_2Zn_2$: 1358.4831; found: 1358.4869; UV/Vis (CH_2Cl_2): $\lambda_{max} = 408$, 536, 571 nm; fluorescence (CH_2Cl_2, $\lambda_{ex} =$ 408 nm): $\lambda_{em} = 577$, 628 nm.

Trimethylene-1,3-dioxy-bridged Zn^{II} diporphyrin B_3: The reaction of **1** (139 mg, 0.24 mmol) and 1,3-dibromopropane (12 μL, 0.12 mmol) in dry acetone (10 mL) in the presence of anhydrous K_2CO_3 (345 mg, 2.4 mmol) gave $\mathbf{B_3}$ (98 mg, 61%) and **4** (32 mg, 21%). $\mathbf{B_3}$: ^{1}H NMR ($CDCl_3$): $\delta = 10.09$ (s, 4H), 9.33 (d, $J = 5$ Hz, 4H), 9.24 (d, $J = 5$ Hz, 4H), 9.17 (d, $J = 4$ Hz, 4H), 9.12 (d, $J = 4$ Hz, 4H), 8.17 (br s, 2H), 8.11 (br s, 2H), 7.90 (br s, 2H), 7.86 (br s, 2H), 7.79 (d, $J = 8$ Hz, 2H), 7.63 (t, $J = 8$ Hz, 2H), 7.36 (d, $J =$ 8 Hz, 2H), 4.47 (t, $J = 6$ Hz, 4H), 2.48 (m, 2H), 1.59 (s, 18H), 1.57 ppm (s, 18H); FAB HRMS: *m*/*z* calcd for $C_{83}H_{76}N_8O_2Zn_2$: 1344.4674; found: 1344.4612; UV/Vis (CH_2Cl_2): $\lambda_{max} = 408$, 537, 574 nm; fluorescence (CH_2Cl_2, $\lambda_{ex} = 408$ nm): $\lambda_{em} = 576$, 628 nm.

5-(3,5-Di-*tert*-butylphenyl)-15-(3,1-propenoxyphenyl)porphyrin (4): ^{1}H NMR ($CDCl_3$): $\delta = 10.31$ (s, 2H), 9.40 (d, $J = 5$ Hz, 2H), 9.39 (d, $J =$ 5 Hz, 2H), 9.13 (d, $J = 5$ Hz, 2H), 9.12 (d, $J = 5$ Hz, 2H), 7.88 (d, $J = 10$Hz, 1H), 7.88 (br s, 1H), 7.85 (t, $J = 2$Hz, 1H), 7.70 (t, $J = 8$ Hz, 2H), 7.39 (dd, $J = 2$, 8 Hz, 2H), 6.19 (m, 1H), 5.53 (d, $J = 1$, 17 Hz, 1H), 5.37 (t, $J =$ 1,10 Hz, 1H), 4.78 (d, 2H), 1.58 (s, 18H), -3.06 ppm (br s, 2H); FAB MS: *m*/*z* calcd for $C_{43}H_{42}N_4O$: 630.34; found: 630.31; UV/Vis (CH_2Cl_2): $\lambda_{max} =$ 408, 538, 575, 632 nm; fluorescence (CH_2Cl_2, $\lambda_{ex} = 408$ nm): $\lambda_{em} = 632$, 695 nm.

Dimethylene-1,2-dioxy-bridged Zn^{II} diporphyrin B_2: Diporphyrin $\mathbf{B_2}$ was prepared from the reaction of **1** (140 mg, 0.24 mmol) and 1,2-dibromoethane (34 μL, 0.39 mmol) in dry DMF (10 mL) in the presence of anhydrous K_2CO_3 (345 mg, 2.4 mmol) in 40% yield (62 mg): ^{1}H NMR ($CDCl_3$): $\delta = 10.05$ (s, 4H), 9.31 (d, $J = 5$ Hz, 4H), 9.20 (d, $J = 4$ Hz, 4H), 9.16 (d, $J = 5$ Hz, 4H), 9.12 (d, $J = 5$ Hz, 4H), 8.17 (br s, 2H), 8.08 (br s, 2H), 7.99 (br s, 2H), 7.85 (br s, 2H), 7.82 (d, $J = 8$ Hz, 2H), 7.67 (t, $J = 8$ Hz, 2H), 7.46 (dd, $J = 2$, 8 Hz, 2H), 4.69 (s, 4H), 1.59 (s, 18H), 1.56 ppm (s, 18H); FAB HRMS: *m*/*z* calcd for $C_{82}H_{74}N_8O_2Zn_2$: 1330.4518; found: 1330.4537; UV/Vis (CH_2Cl_2): $\lambda_{max} = 407$, 536, 572 nm; fluorescence (CH_2Cl_2, $\lambda_{ex} =$ 408 nm): $\lambda_{em} = 576$, 627 nm.

3,5-Di-*tert*-butylphenyl)-15-(3-vinyloxyphenyl)porphyrin (3): The reaction of **1** (139 mg, 0.24 mmol) and 1,2-dibromoethane (12 μL, 0.12 mmol) in dry acetone (10 mL) in the presence of anhydrous K_2CO_3 (345 mg, 2.4 mmol) for 24 h gave **3** in 10% yield (~10 mg) at 16% conversion of **1**. Only a trace amount of $\mathbf{B_2}$ was detected in this reaction. **3**: ^{1}H NMR ($CDCl_3$): $\delta = 10.32$ (s, 2H), 9.41 (d, $J = 5$ Hz, 2H), 9.40 (d, $J = 5$ Hz, 2H), 9.14 (d, $J = 5$ Hz, 2H), 9.10 (d, $J = 5$ Hz, 2H), 8.14 (d, $J = 2$ Hz, 2H), 8.01 (d, $J = 7$ Hz, 1H), 7.95 (br s, 1H), 7.85 (t, $J = 2$Hz, 1H), 7.75 (t, $J = 8$ Hz, 1H), 7.48 (dd, $J = 2$, 8 Hz, 1H), 6.95 (dd, $J = 6$, 14 Hz, 1H), 4.96 (dd, $J = 1$, 15 Hz, 1H), 4.54 (dd, $J = 1$, 5 Hz, 1H), 1.58 (s, 18H), -3.06 ppm (br s, 2H); FAB MS: *m*/*z* calcd for $C_{42}H_{40}N_4O$: 616.32; found: 617; UV/Vis (CH_2Cl_2): $\lambda_{max} = 408$, 538, 575, 632 nm; fluorescence (CH_2Cl_2, $\lambda_{ex} = 408$ nm): $\lambda_{em} = 632$, 695 nm.

Methylene-1,1-dioxy-bridged Zn^{II} diporphyrin B_1: Diporphyrin $\mathbf{B_1}$ was prepared from the reaction of **1** (100 mg, 0.17 mmol) and dibromomethane (19 μL, 0.27 mmol) in dry DMF (10 mL) in the presence of anhydrous

  0947-6539/03/0901-0073 $ 20.00+.50/0

K_2CO_3 (244 mg, 1.7 mmol) in 84% yield (95 mg): ^{1}H NMR ($CDCl_3$): $\delta =$ 9.76 (s, 4H), 9.17 (d, $J = 5$ Hz, 4H), 9.11 (d, $J = 4$ Hz, 4H), 9.04 (d, $J = 5$ Hz, 4H), 8.97 (d, $J = 5$ Hz, 4H), 8.29 (brs, 2H), 8.28 (brs, 2H), 7.96 (brs, 2H), 7.84 (brs, 2H), 7.81 (d, $J = 8$ Hz, 2H), 7.71 (t, $J = 8$ Hz, 2H), 7.32 (d, $J =$ 8 Hz, 2H), 6.25 (s, 4H), 1.62 (s, 18H), 1.56 ppm (s, 18H); FAB HRMS: *m/z* calcd for $C_{82}H_{72}N_8O_2Zn_2$: 1316.4361; found: 1316.4358; UV/Vis (CH_2Cl_2): $\lambda_{max} = 407$, 412 (shoulder), 536, 572 nm; fluorescence (CH_2Cl_2, $\lambda_{ex} =$ 408 nm): $\lambda_{em} = 576$, 627 nm.

General procedure for preparation of S_n: A flask containing a solution of B_n in $CHCl_3$ was covered with foil, and a solution of $AgPF_6$ in CH_3CN (0.13 mM) was added. After stirring for 2 h, the reaction mixture was washed with water and brine, and was dried over anhydrous Na_2SO_4. A solution of $Zn(OAc)_2$ in methanol (1–2 mL) was added, and the resulting solution was stirred at room temperature for 1 h. Then the reaction mixture was again washed with water and brine, and dried over anhydrous Na_2SO_4, and evaporated. The product separation was performed on a preparative GPC (BioRad Bio-Beads SX-1 packed in toluene). The first and second fractions contained *meso–meso*-coupled higher oligomers and the last one contained S_n and B_n, which was separated by recycling GPC-HPLC with $CHCl_3$ as an eluent. The *meso–meso*-strapped diporphyrin S_n was obtained after recrystallization from CH_2Cl_2/hexane.

Decamethylene-1,10-dioxy-strapped *meso–meso*–linked Zn^{II} diporphyrin S_{10}: Diporphyrin B_{10} (60, mg 42 μmol) in $CHCl_3$ (450 mL) gave dimer S_{10} by the general method in 68% yield (41 mg): ^{1}H NMR ($CDCl_3$): $\delta = 10.39$ (s, 2H), 9.50 (d, $J = 5$ Hz, 2H), 9.49 (d, $J = 4$ Hz, 2H), 9.21 (d, $J = 5$ Hz, 2H), 9.21 (d, $J = 4$ Hz, 2H), 8.79 (d, $J = 5$ Hz, 2H), 8.70 (d, $J = 5$ Hz, 2H), 8.30 (d, $J = 5$ Hz, 2H), 8.20 (t, $J = 2$ Hz, 2H), 8.05 (t, $J = 2$ Hz, 2H), 7.95 (d, $J =$ 5 Hz, 2H), 7.90 (d, $J = 8$ Hz, 2H), 7.74 (d, $J = 2$ Hz, 2H), 7.73 (t, $J = 2$ Hz, 2H), 7.57 (t, $J = 8$ Hz, 2H), 7.20 (dd, $J = 3$, 9 Hz, 2H), 4.12 (m, 2H), 4.09 (m, 2H), 1.76 (m, 4H), 1.49 (s, 18H), 1.44 (s, 18H), 1.31–1.34 (m, 8H), 0.92 ppm (m, 4H); FAB HRMS: *m/z* calcd for $C_{90}H_{88}N_8O_2Zn_2$: 1440.5613; found: 1440.5520; UV/Vis (CH_2Cl_2): λ_{max} ($\log\varepsilon$) = 414 (5.41), 447 (5.33), 553 nm (4.72); fluorescence (CH_2Cl_2, $\lambda_{ex} = 414$ nm): $\lambda_{em} = 651$ nm.

Octamethylene-1,8-dioxy-strapped *meso–meso*-linked Zn^{II} diporphyrin S_8: Diporphyrin B_8 (4,0 mg 28 μmol) in $CHCl_3$ (200 mL) gave dimer S_8 by the general method in 65% yield (26 mg): ^{1}H NMR ($CDCl_3$): $\delta = 10.39$ (s, 2H), 9.51 (d, $J = 4$ Hz, 2H), 9.50 (d, $J = 4$ Hz, 2H), 9.26 (d, $J = 5$ Hz, 2H), 9.21 (d, $J = 4$ Hz, 2H), 8.84 (d, $J = 5$ Hz, 2H), 8.66 (d, $J = 5$ Hz, 2H), 8.43 (d, $J = 4$ Hz, 2H), 8.24 (s, 2H), 8.04 (s, 2H), 7.96 (d, $J = 8$ Hz, 2H), 7.86 (d, $J =$ 5 Hz, 2H), 7.74 (t, $J = 3$ Hz, 2H), 7.60 (t, $J = 8$ Hz, 2H), 7.22 (dd, $J = 2$, 8Hz, 2H), 4.09 (m, 2H), 4.02 (m, 2H), 1.79 (m, 4H), 1.6–1.4 (m, 8H), 1.53 ppm (s, 36H); FAB HRMS: *m/z* calcd for $C_{88}H_{84}N_8O_2Zn_2$: 1412.5300; found: 1412.5232; UV/Vis (CH_2Cl_2): λ_{max} ($\log\varepsilon$) = 415 (5.39), 447 (5.29), 554 nm (4.68); fluorescence (CH_2Cl_2, $\lambda_{ex} = 415$ nm): $\lambda_{em} = 623$, 652 nm.

Hexamethylene-1,6-dioxy-strapped *meso–meso*-linked Zn^{II} diporphyrin S_6: Diporphyrin B_6 (40 mg, 29 μmol) in $CHCl_3$ (200 mL) gave dimer S_6 by the general method in 60% yield (24 mg): ^{1}H NMR ($CDCl_3$): $\delta = 10.37$ (s, 2H), 9.50 (d, $J = 5$ Hz, 4H), 9.33 (d, $J = 5$ Hz, 2H), 9.21 (d, $J = 5$ Hz, 2H), 8.89 (d, $J = 5$ Hz, 2H), 8.62 (d, $J = 5$ Hz, 2H), 8.61 (d, $J = 5$ Hz, 2H), 8.28 (brs, 2H), 8.06 (d, $J = 6$ Hz, 2H), 7.76 (brs, 2H), 7.74 (brs, 2H), 7.71 (d, $J =$ 5 Hz, 2H), 7.64 (t, $J = 8$ Hz, 2H), 7.24 (dd, $J = 3$, 8 Hz, 2H), 4.07 (m, 2H), 3.99 (m, 2H), 1.88 (m, 4H), 1.6–1.5 (m, 4H), 1.56 (s, 18H), 1.44 ppm (s, 18H); FAB HRMS: *m/z* calcd for $C_{86}H_{80}N_8O_2Zn_2$: 1384.4987; found: 1384.4910; UV/Vis (CH_2Cl_2): λ_{max} ($\log\varepsilon$) = 416 (5.39), 448 (5.29), 555 nm (4.70); fluorescence (CH_2Cl_2, $\lambda_{ex} = 416$ nm): $\lambda_{em} = 628$, 654 nm.

Pentamethylene-1,5-dioxy-strapped *meso–meso*-linked Zn^{II} diporphyrin S_5: Diporphyrin B_5 (20 mg, 60 μmol) in $CHCl_3$ (200 mL) gave dimer S_5 by the general method in 43% yield (26 mg): ^{1}H NMR ($CDCl_3$): $\delta = 10.36$ (s, 2H), 9.50 (d, $J = 5$ Hz, 4H), 9.38 (d, $J = 5$ Hz, 2H), 9.23 (d, $J = 5$ Hz, 2H), 8.98 (d, $J = 5$ Hz, 2H), 8.85 (d, $J = 5$ Hz, 2H,), 8.55 (d, $J = 5$ Hz, 2H), 8.37 (brs, 2H), 8.15 (d, $J = 8$ Hz, 2H), 8.03 (brs, 2H), 7.79 (brs, 2H), 7.67 (t, $J =$ 8 Hz, 2H), 7.65 (brs, 2H), 7.60 (d, $J = 5$ Hz, 2H), 7.22 (dd, $J = 2$, 8 Hz, 2H), 4.20 (m, 2H), 4.03 (m, 2H), 1.97(m, 2H), 1.88 (m, 2H), 1.61 (s, 18H), 1.59 (m, 2H), 1.46 ppm (s, 18H); FAB HRMS: *m/z* calcd for $C_{85}H_{78}N_8O_2Zn_2$: 1370.4831; found: 1370.4916; UV/Vis (CH_2Cl_2): λ_{max} ($\log\varepsilon$) = 417 (5.35), 450 (5.21), 537, 559 nm (4.67); fluorescence (CH_2Cl_2, $\lambda_{ex} = 417$ nm): $\lambda_{em} =$ 626, 657 nm.

Tetramethylene-1,4-dioxy-strapped *meso–meso*–linked Zn^{II} diporphyrin S_4: Diporphyrin B_4 (40 mg 29 μmol) in $CHCl_3$ (300 mL) gave dimer S_4 by the general method in 63% yield (25 mg): ^{1}H NMR ($CDCl_3$): $\delta = 10.36$ (s, 2H), 9.51 (d, $J = 5$ Hz, 2H), 9.50 (d, $J = 5$ Hz, 2H), 9.43 (d, $J = 5$ Hz, 2H), 9.25 (d, $J = 5$ Hz, 2H), 9.22 (d, $J = 5$ Hz, 2H), 9.08 (d, $J = 5$ Hz, 2H), 8.45 (d, $J = 5$ Hz, 2H), 8.38 (brs, 2H), 8.15 (d, $J = 7$ Hz, 2H), 8.08 (brs, 2H), 7.81 (brs, 2H), 7.67 (t, $J = 8$ Hz, 2H), 7.65 (brs, 2H), 7.25 (dd, $J = 3$, 8 Hz, 2H), 7.18 (d, $J = 5$ Hz, 2H), 4.14 (m, 2H), 3.94 (m, 2H), 2.17 (m, 2H), 2.03 (m, 2H), 1.62 (s, 18H), 1.47 ppm (s, 18H); FAB HRMS: *m/z* calcd for $C_{84}H_{76}N_8O_2Zn_2$: 1356.4674; found: 1356.4752; UV/Vis (CH_2Cl_2): λ_{max} ($\log\varepsilon$) = 419 (5.30), 451 (5.16), 538 (4.44), 560 nm (4.64); fluorescence (CH_2Cl_2, $\lambda_{ex} = 419$ nm): $\lambda_{em} = 628$, 659 nm.

Trimethylene-1,3-dioxy-strapped *meso–meso*-linked Zn^{II} diporphyrin S_3: Diporphyrin B_3 (40 mg 30 μmol) in $CHCl_3$ (300 mL) gave dimer S_3 by the general method in 38% yield (15 mg): ^{1}H NMR ($CDCl_3$): $\delta = 10.33$ (s, 2H), 9.48 (d, $J = 4$ Hz, 6H), 9.44 (d, $J = 5$ Hz, 2H), 9.23 (d, $J = 5$ Hz, 2H), 9.13 (d, $J = 5$ Hz, 2H), 8.44 (brs, 2H), 8.34 (d, $J = 5$ Hz, 2H), 8.31 (d, $J = 7$ Hz, 2H), 8.03 (brs, 2H), 7.82 (brs, 2H), 7.72 (t, $J = 8$ Hz, 2H), 7.50 (brs, 2H), 7.25 (dd, $J = 2$, 8 Hz, 2H), 6.90 (d, $J = 5$ Hz, 2H), 4.57 (m, 2H), 4.13 (m, 2H), 2.46 (m, 2H), 1.65 (s, 18H), 1.47 ppm (s, 18H); FAB HRMS: *m/z* calcd for $C_{83}H_{74}N_8O_2Zn_2$: 1342.4518; found: 1342.4493; UV/Vis (CH_2Cl_2): λ_{max} ($\log\varepsilon$) = 420 (5.28), 469 (5.14), 538 (4.47), 564 nm (4.62); fluorescence (CH_2Cl_2, $\lambda_{ex} = 420$ nm): $\lambda_{em} = 636$ nm.

Dimethylene-1,2-dioxy-strapped *meso–meso*-linked Zn^{II} diporphyrin S_2: Diporphyrin B_2 (20 mg 15 μmol) in $CHCl_3$ (200 mL) gave dimer S_2 by the general method in 35% yield (7 mg): ^{1}H NMR ($CDCl_3$): $\delta = 10.32$ (s, 2H), 9.91 (d, $J = 4$ Hz, 2H), 9.49 (d, $J = 5$ Hz, 4H), 9.46 (d, $J = 5$ Hz, 2H), 9.24 (d, $J = 4$ Hz, 2H), 9.23 (d, $J = 5$ Hz, 2H), 8.44 (brs, 2H), 8.27 (d, $J = 8$ Hz, 2H), 8.10 (brs, 2H), 8.10 (d, $J = 5$ Hz, 2H), 7.85 (brs, 2H), 7.69 (t, $J = 8$ Hz, 2H), 7.48 (brs, 2H), 7.25 (dd, $J = 2$, 8 Hz, 2H), 6.32 (d, $J = 5$ Hz, 2H), 4.73 (m, 2H), 4.39 (m, 2H), 1.67 (s, 18H), 1.51 ppm (s, 18H); FAB HRMS: *m/z* calcd for $C_{82}H_{72}N_8O_2Zn_2$: 1328.4361; found: 1328.4423; UV/Vis (CH_2Cl_2): λ_{max} ($\log\varepsilon$) = 399 (5.18), 422 (5.25), 473 (5.16), 539 (4.53), 566 nm (4.61); fluorescence (CH_2Cl_2, $\lambda_{ex} = 422$ nm): $\lambda_{em} = 648$ nm.

Methylene-1,1-dioxy-strapped *meso–meso*-linked Zn^{II} diporphyrin S_1: Diporphyrin B_1 (40 mg 15 μmol) in $CHCl_3$ (800 mL) gave dimer S_1 by the general method in 20% yield (8 mg): ^{1}H NMR ($CDCl_3$): $\delta = 10.31$ (s, 2H), 10.08 (d, $J = 4$ Hz, 2H), 9.48 (brs, 6H), 9.26 (d, $J = 5$ Hz, 2H), 9.23 (d, $J =$ 4 Hz, 2H), 8.55 (d, $J = 8$ Hz, 2H), 8.46 (brd, 2H), 8.13 (d, $J = 4$ Hz, 2H), 8.08 (brs, 2H), 7.87 (brs, 2H), 7.82 (t, $J = 8$ Hz, 2H), 7.51 (brs, 2H), 7.43 (d, $J = 8$ Hz, 2H), 6.12 (d, $J = 5$ Hz, 2H), 5.98 (s, 2H), 1.69 (s, 18H), 1.51 ppm (s, 18H); FAB HRMS: *m/z* calcd for $C_{81}H_{70}N_8O_2Zn_2$: 1314.4205; found: 1314.4388; UV/Vis (CH_2Cl_2): $\lambda_{max} = 395$, 424, 478, 540, 572 nm; fluorescence (CH_2Cl_2, $\lambda_{ex} = 424$ nm): $\lambda_{em} = 658$ nm.

CCDC-188525 (**2Cu**), CCDC-188526 (**S_8Cu**), CCDC-188527 (**S_4Cu**), and CCDC-188528 (**S_2Cu**) contain the supplementary crystallographic data for this paper. These data can be obtained free of charge via www.ccdc.cam.ac.uk/conts/retrieving.html (or from the Cambridge Crystallographic Data Centre, 12 Union Road, Cambridge CB2 1EZ, UK; fax: (+44) 1223-336-033; or e-mail: deposit@ccdc.cam.ac.uk).

Acknowledgements

This work was supported by Grant-in-Aid for Scientific Research (No.11223205 and No.12440196) from the Ministry of Education, Science, Sports and Culture of Japan. The work at Yonsei university was financially supported by the creative research initiatves program of the Ministry of Science and Technology of Korea (MOST). We are grateful to Prof. H. Tamiaki (Ritsumeikan University) and Dr. T. Miyatake of (Ryukoku University) for the CD measurements, and Mr. Seong Moon Jang for Raman measurements. N.Y. is grateful for a JSPS Research Fellowship for Young Scientists.

[1] a) J. P. Collman, F. C. Anson, C. E. Barnes, C. S. Bencosme, T. Geiger, E. R. Evitt, R. P. Kreh, K. Meier, R. B. Pettman, *J. Am. Chem. Soc.* **1983**, *105*, 2694; b) C. K. Chang, I. Abdalmuhdi, *J. Org. Chem.* **1983**, *48*, 5388.

[2] a) F. P. Schwarz, M. Gouterman, Z. Muljiani, D. H. Dolphin, *Bioinorg. Chem.* **1972**, *2*, 1; b) J. A. Anton, P. A. Loach, Govindjee, *Photochem. Photobiol.* **1978**, *28*, 235; c) I. Tabushi, T. Sasaki, *Tetrahedron Lett.* **1982**, *23*, 1913.

  0947-6539/03/0901-0074 $ 20.00+.50/0 *Chem. Eur. J.* **2003**, *9*, No. 1

[3] a) M. R. Wasielewski, *Chem. Rev.* **1992**, *92*, 435; b) A. Osuka, N. Mataga, T. Okada, *Pure Appl. Chem*. **1997**, *69*, 797; c) J.-H. Chou, H. S. Nalwa, M. E. Kosal, N. A. Rakow, K. S. Suslick, in *The Porphyrin Handbook, Vol. 6* (Eds.: K. M. Kadish, K. M. Smith, R. Guilard) Academic Press, San Diego, **2000**, Chapter 41.
[4] a) J. L. Sesslar, M. R. Johnson, T.-Y. Ling, S. E. Creager, *J. Am. Chem. Soc.* **1988**, *110*, 3659; b) K. Maruyama, A. Osuka, *Pure Appl. Chem*. **1990**, *62*, 1511; c) J. M. Zaleski, C. K. Chang, G. E. Leroi, R. I. Cukier, D. G. Nocera, *J. Am. Chem. Soc.* **1992**, *114*, 3564; d) T. L. Netzel, M. A. Bergkamp, C. K. Chang, *J. Am. Chem. Soc.* **1982**, *104*, 1952.
[5] M. R. Wasielewski, in *Photoinduced Electron Transfer* (Eds.: M. A. Fox, M. Chanon), Elsevier, Amsterdam, **1988**, Chapter 1.4.
[6] A. Helms, D. Heiler, G. McLendon, *J. Am. Chem. Soc*. **1991**, *113*, 4325.
[7] A. Osuka, J. Shin, R. Yoneshima, H. Shiratori, T. Ohno, K. Nozaki, Y. Nishimura, I. Yamazaki, S. Taniguchi, T. Shimizu, T. Okada, *J. Porphyrins Phthalocyanines* **1999**, *3*, 729.
[8] a) A. Osuka, K. Maruyama, *J. Am. Chem. Soc.* **1988**, *110*, 4454. The exciton coupling of other covalently linked diporphyrins; see Refs. [2b,c] and b) B. von Maltzan, *Z. Naturforsch. Teil A* **1985**, *40*, 389; c) J. L. Sessler, J. Hugdahl, M. R. Johnson, *J. Org. Chem.* **1986**, *51*, 2838; d) H. Meier, Y. Kobuke, S. Kugimiya, *J. Chem. Soc. Chem. Commun.* **1989**, 923.
[9] a) A. Osuka, K. Maruyama, I. Yamazaki, N. Tamai, *Chem. Phys. Lett.* **1990**, *165*, 392; b) A. Osuka, K. Marumaya, N. Mataga, T. Asahi, I. Yamazaki, N. Tamai, *J. Am. Chem. Soc.* **1990**, *112*, 4958.
[10] a) S. Matile. N. Berova, K. Nakanishi, S. Novkova, I. Philipova, B. Blagoev, *J. Am. Chem. Soc.* **1995**, *117*, 7021; b) X. Huang, B. H. Rickman, B. Borhan, N. Berova, K. Nakanishi, *J. Am. Chem. Soc.* **1998**, *120*, 6185; c) V. V. Borovkov, J. M. Lintuluoto, M. Fujiki, Y. Inoue, *J. Am. Chem. Soc.* **2000**, *122*, 4403.
[11] a) A. Osuka, H. Shimidzu, *Angew. Chem.* **1997**, *109*, 93; *Angew. Chem. Int. Ed. Engl.* **1997**, *36*, 135; b) T. Ogawa, Y. Nishimoto, N. Yoshida, N. Ono, A. Osuka, *Chem. Commun*. **1998**, 337; c) T. Ogawa, Y. Nishimoto, N. Yoshida, N. Ono, A. Osuka, *Angew. Chem.* **1999**, *111*, 140; *Angew. Chem. Int. Ed.* **1999**, *38*, 176; d) N. Aratani, A. Osuka, Y. H. Kim, D. H. Jeong, D. Kim, *Angew. Chem.* **2000**, *112*, 1517; *Angew. Chem. Int. Ed.* **2000**, *39*, 1458; e) H. S. Cho, N. W. Song, Y. H. Kim, S. C. Jeoung, S. Hahn, D. Kim, S. K. Kim, N. Yoshida, A. Osuka, *J. Phys. Chem. B* **2000**, *104*, 3287; f) A. A. Bhuiyan, J. Seth, N. Yoshida, A. Osuka, D. F. Bocian, *J. Phys. Chem. A* **2000**, *104*, 10757; g) Y. H. Kim, D. H. Jeong, D. Kim, S. C. Jeoung, H. S. Cho, S. K. Kim, N. Aratani, A. Osuka, *J. Am. Chem. Soc.* **2001**, *123*, 76.
[12] Several groups reported independently the synthesis of *meso*–*meso*-coupled diporphyrins: a) K. Susumu, T. Shimidzu, K. Tanaka, H. Segawa, *Tetrahedron Lett*. **1996**, *37*, 8399; b) R. G. Khoury, L. Jaquinod, K. M. Smith, *Chem. Commun*. **1997**, 1057; c) M. O. Senge, X. Feng, *Tetrahedron Lett*. **1999**, *40*, 4165; d) X. Shi, L. S. Liebeskind, *J. Org. Chem*. **2000**, *65*, 1665.
[13] a) M. Goutermann, *J. Mol. Spectrosc*. **1961**, *6*, 138; b) M. Kasha, H. R. Rawls, M. A. El-Bayoumi, *Pure Appl. Chem*. **1965**, 11, 371.
[14] H. S. Cho, D. H. Jeong, M. C. Yoon, Y. H. Kim, Y. R. Kim, D. Kim, S. C. Jeoung, S. K. Kim, N. Aratani, H. Shinmori, A. Osuka, *J. Phys. Chem. A* **2001**, *105*, 4200.
[15] A preliminary short report of the present work has been published: N. Yoshida, A. Osuka, *Org. Lett.* **2000**, *2*, 2963.
[16] N. Yoshida, A. Osuka, *Tetrahedron Lett.* **2000**, *41*, 9287.
[17] We have obtained X-ray crystal structures of other nonstrapped Zn^{II} diporphyrins which have dihedral angles of nearly 90°: N. Aratani, A. Osuka, unpublished results.
[18] N. Yoshida, N. Aratani, A. Osuka, *Chem. Commun*. **2000**, 197.
[19] P. G. Seybold, M. Goutermann, *J. Mol. Spectrosc.* **1969**, *31*, 1.
[20] a) X.-Y. Li, R. S. Czernuszewicz, J. R. Kincaid, Y. O. Su, T. G. Spiro, *J. Phys. Chem.* **1990**, *94*, 31; b) D. H. Jeong, M.-C. Yoon, S. M. Jang, D. Kim, D. W. Cho, N. Yoshida, N. Aratani, A. Osuka, *J. Phys. Chem. A* **2002**, *106*, 2359.
[21] N. Ohta, Y. Iwaki, T. Ito, I. Yamazaki, A. Osuka, *J. Phys. Chem. B* **1999**, *103*, 11242.
[22] a) T. P. Wijesekera, J. B. Paine III, D. Dolphin, F. W. B. Einstein, T. Jones, *J. Am. Chem. Soc.* **1983**, *105*, 6747; b) M. Momenteau, J. Mispelter, B. Loock, E. Bisagni, *J. Chem. Soc. Perkin Trans. 1* **1983**, 189; c) U. Simonis, F. A. Walker, P. L. Lee, B. J. Hanquet, D. J. Meyerhoff, W. R. Scheidt, *J. Am. Chem. Soc.* **1987**, *109*, 2659.
[23] S. F. Mason, R. H. Seal, D. R. Roberts, *Tetrahedron* **1974**, *30*, 1671.
[24] O. Bilsel, J. Rodriguez, S. N. Milam, P. A. Gorlin, G. S. Girolami, K. S. Suslick, D. Holten, *J. Am. Chem. Soc.* **1992**, *114*, 6528.
[25] J. D. Petke, G. M. Maggiora, *J. Chem. Phys.* **1986**, *84*, 1640.
[26] M. J. Frisch, G. W. Trucks, H. B. Schlegel, G. E. Scuseria, M. A. Robb, J. R. Cheeseman, V. G. Zakrzewski, J. A. Montgomery, R. E. Stratmann, J. C. Burant, S. Dapprich, J. M. Millam, A. D. Daniels, K. N. Kudin, M. C. Strain, O. Farkas, J. Tomasi, V. Barone, M. Cossi, R. Cammi, B. Mennucci, C. Pomelli, C. Adamo, S. Clifford, J. Ochterski, G. A. Petersson, P. Y. Ayala, Q. Cui, K. Morokuma, D. K. Malick, A. D. Rabuck, K. Raghavachari, J. B. Foresman, J. Cioslowski, J. V. Ortiz, A. G. Baboul, B. B. Stefanov, G. Liu, A. Liashenko, P. Piskorz, I. Komaromi, R. Gomperts, R. L. Martin, D. J. Fox, T. Keith, M. A. Al-Laham, C. Y. Peng, A. Nanayakkara, C. Gonzalez, M. Challacombe, P. M. W. Gill, B. Johnson, W. Chen, M. W. Wong, J. L. Andres, C. Gonzalez, M. Head-Gordon, E. S. Replogle, J. A. Pople, Gaussian 98, Revision A.7, Gaussian, Pittsburgh, PA, **1998**.
[27] J. Almlöf, T. H. Fischer, P. G. Gassman, A. Ghosh, M. Häser, *J. Phys. Chem.* **1993**, *97*, 10964.
[28] R. Ditchfield, W. J. Hehre, J. A. Pople, *J. Chem. Phys.* **1971**, *54*, 724.
[29] S. Huzinaga, J. Andzelm, M. Klobukowski, E. Radzio-Andzelm, Y. Sakai, H. Tatewaki, *Gaussian Basis Sets for Molecular Calculations*, Elsevier, New York, **1984**.
[30] J. E. Ridley, M. C. Zerner, *Theor. Chim. Acta* **1973**, *32*, 111.
[31] K. Nishimoto, N. Mataga, *Z. Phys. Chem.* **1957**, *12*, 335.
[32] B. J. Orr, J. F. Ward, *Mol. Phys.* **1971**, *20*, 513.
[33] S. Mukamel, S. Tretiak, T. Wagersreiter, V. Chernyak, *Science* **1997**, *277*, 781.
[34] M. Gouterman, *J. Chem. Phys.* **1959**, *30*, 1139.

Received: July 26, 2002 [F4287]

  0947-6539/03/0901-0075 $ 20.00+.50/0